

Superradiant phase transition in an atom-cavity system combined with intracavity parametric down-conversion

Deshui Yu and Sam Genway*

School of Physics and Astronomy, The University of Nottingham, Nottingham NG7 2RD, United Kingdom

(Received 18 June 2014; published 15 October 2014)

We study an atom-cavity system composed of an ensemble of three-level atoms interacting with a high-finesse single-mode optical resonator. Two examples of physical models, the laser-driven Λ -type atomic system and the three-level ladder-type atomic system, are investigated in detail. By altering the collective atom-cavity dynamics via an intracavity optical parametric amplification process, a spin-boson model is realized when the composite system operates in the far-detuning regime. When the number of atoms exceeds a critical value, the quantum system undergoes a superradiant phase transition whose dependence on different experimentally adjustable parameters is explored in detail. The effects of the spontaneous emission of atoms and the cavity loss on the phase transition are considered, and measuring the cavity output field itself gives an experimental probe of the superradiant phase transition.

DOI: [10.1103/PhysRevA.90.043824](https://doi.org/10.1103/PhysRevA.90.043824)

PACS number(s): 37.30.+i, 42.50.Pq, 05.70.Fh

I. INTRODUCTION

Superradiant phase transitions have been of interest for many years [1–5]. Captured in their simplest form by the Dicke Hamiltonian [6], the phase transition occurs when the coupling between a set of two-level atoms and an optical mode is increased above a critical threshold; beyond this, the optical mode becomes macroscopically populated and a dramatic and collective change to the atoms' electronic states occurs [7,8]. In its original context, the Dicke model has not been realized experimentally. However, an equivalent quantum phase transition has been observed [9,10] in a system involving a Bose-Einstein condensate (BEC) trapped inside a high-finesse optical cavity transversely driven by an external standing-wave pump laser [11–13]. When the pump power exceeds a critical value, the BEC undergoes a transition to a spatially self-organized phase.

Nevertheless, a practical realization of a Dicke phase transition for real atoms in a cavity remains as a challenge: it is impossible to realize the so-called counter-rotating terms in the usual Dicke Hamiltonian [1], due to the fact that the energy splitting between two involved atomic levels and cavity-mode frequency dramatically exceed the atomic dipole coupling strength [14]. Furthermore, in practice, unavoidable atomic spontaneous emission and cavity loss irreversibly break the unitary time evolution such that open-quantum-system extensions to the Dicke model should be explored.

A promising route to the Dicke phase transition has been proposed in Ref. [15], where a large number of laser-driven three-level Λ -type atoms are strongly coupled to a high-finesse cavity. By setting both driving-field and cavity-mode frequencies far-off-resonant to their corresponding atomic transitions, respectively, the influence of atomic spontaneous emission can be sufficiently suppressed [16] and the energy separation of two involved atomic levels in the traditional Dicke model is significantly reduced to the energy splitting of two ground-state hyperfine levels. Moreover, since the system works in the strong-coupling regime, the optical resonator

interacts with atoms for many times before the cavity loss happens. Consequently, the effective atom-cavity interaction in the usual Dicke model is strong enough that the phase transition regime can be reached for the real atoms [17,18].

Along this promising route [15], we explore a more rich composite system composed of an ensemble of laser-driven three-level Λ -type atoms interacting with a single-mode optical resonator in Sec. II. We employ the nonlinear process of intracavity laser-driven degenerate parametric down-conversion to obtain an effective Dicke-like model in the far-detuned regime of the atom-light field and atom-cavity interactions. We find that a superradiant quantum phase transition occurs when the number of atoms is larger than a critical value. The relation of this phase transition to the nonlinear parametric oscillation and other experimentally tunable parameters is discussed in detail. We further study the dependence of the phase transition on the unavoidable cavity dissipation and find the superradiant phase transition is marked by a significant amplification of the quadrature fluctuations of the cavity output field around the critical point.

Our physical model provides an alternative approach to access the Dicke-like model for real atoms in experiment, which is of benefit to the experimental diversity, for example, improving the adjustable freedoms of different physical parameters. Besides, introducing the nonlinear optics into the collective atom-cavity dynamics leads to interesting and unpredictable results, which are very different from those predicted in the traditional Dicke model [1] and an optical cavity-quantum-electrodynamics system [15]. Some examples of these results are the following. (i) For a nondissipative system only the atomic excitation branch is valid in both normal and superradiant phases while both atomic and photonic excitation branches are valid for a dissipative systems. (ii) Enlarging the cavity loss rate can reduce the threshold of the superradiant phase transition in the dissipative case.

In Sec. III, we further explore another atom-cavity composite system, where an ensemble of three-level ladder-type atoms collectively interacting with a single-mode optical cavity, combined with the intracavity parametric down-conversion. We are motivated by the fact that the total transition strength (rate) of a multiphoton process is proportional to the product

*Sam.Genway@gmail.com

of the transition strengths of different one-photon processes. Due to the cavity mode simultaneously coupling two atomic transitions, the collective atom-cavity interaction strength is strongly enhanced by a factor of \sqrt{N} compared with that in the Λ -type system, which results in a significant reduction of the threshold of the phase transition. Like in Sec. II, both nondissipative and dissipative cases are discussed in detail and the spectroscopic properties of the output field are studied as well in Sec. III.

Finally, we give our conclusions and summarize the similarities and differences between those two physical models in Sec. IV.

II. Λ -TYPE ATOMIC SYSTEM

In this section, we consider a composite atom-cavity system, where the collective interaction between a large number of three-level Λ -type atoms and a single-mode optical cavity is modulated by an intracavity laser-driven nonlinear parametric process. We first establish the physical model and then investigate the possible superradiant phase transition in an ideal system where no dissipation is involved. Finally, we study the influence of the unavoidable cavity loss on the phase transition from the spectrum of the cavity output field.

A. Physical model

A one-dimensional chain of lattice-trapped three-level Λ -type atoms is placed inside a high-finesse single-mode optical resonator as shown in Fig. 1. All atoms are equally separated and localized at the cavity standing-wave antinodes. An external laser field at frequency ω_c propagating perpendicular to the atomic chain is applied to couple the one-photon $|1\rangle - |3\rangle$ transition (frequency $\omega_{3,1}$) with a Rabi frequency Ω and a detuning $\Delta_c = \omega_c - \omega_{3,1}$. The single-mode cavity at frequency ω_l interacts with the other leg of the Λ -type system, i.e., the atomic $|2\rangle - |3\rangle$ transition (frequency $\omega_{3,2}$), with a detuning $\Delta_p = \omega_l - \omega_{3,2}$. A nonlinear medium pumped by an extra field is inserted inside the resonator so as to introduce a degenerate parametric down-conversion [19], i.e., the medium converts a pump-field photon at frequency $2\omega_l$ into a pair of identical intracavity photons at frequency ω_l , into the atom-cavity dynamics.

To our best knowledge, this physical system was first discussed in Ref. [20], where the external field used to pump the nonlinear crystal was also treated as a cavity-field mode and the optical bistability in the intracavity-field intensity versus pumping intensity was predicted. In our system, the pump field is considered to be a classical field in the parametric approximation [21].

In the rotating-wave approximation (RWA) and under phase-matching conditions, the Hamiltonian describing a degenerate parametric amplification process and atoms simultaneously interacting with an external driving field and a single-mode cavity is

$$\begin{aligned} \hat{H}/\hbar = & \Delta_c \hat{J}_{1,1} + \Delta_p \hat{J}_{2,2} + \beta(\hat{a}^\dagger \hat{a}^\dagger + \hat{a} \hat{a}) \\ & + \Omega(\hat{J}_{1,3}^\dagger + \hat{J}_{1,3}) + g(\hat{J}_{2,3}^\dagger \hat{a} + \hat{a}^\dagger \hat{J}_{2,3}), \end{aligned} \quad (1)$$

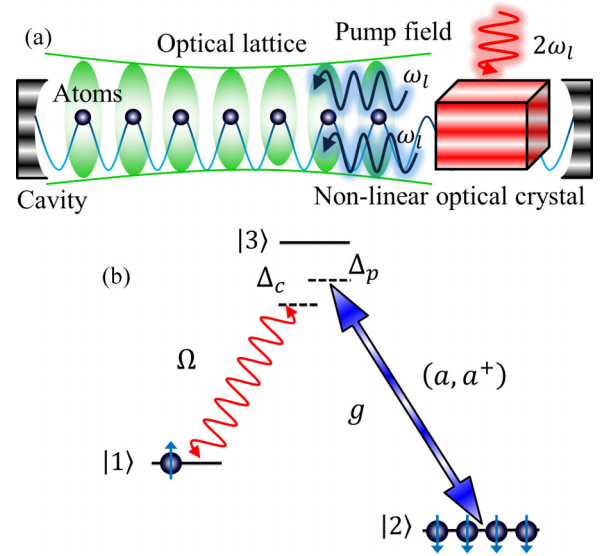


FIG. 1. (Color online) (a) Schematic of the composite atom-cavity system. A bunch of atoms tightly confined in a one-dimensional optical lattice are placed inside a single-mode optical resonator. Each lattice site contains only one atom, which is localized at the standing-wave antinode of the cavity mode. An external laser field traveling in a perpendicular direction to the cavity axis is applied to excite atoms. A nonlinear crystal driven by a classical pump field is inserted inside the optical cavity so as to introduce the degenerate parametric down-conversion process into the atom-cavity dynamics. (b) A three-level Λ -type atomic system composed of $|1, 2, 3\rangle$ states. The external laser field couples to the $|1\rangle - |3\rangle$ transition with a Rabi frequency Ω and detuning Δ_c while the optical cavity interacts with atoms via the $|2\rangle - |3\rangle$ transition with a coupling strength of g and detuning Δ_p .

where the collective atomic operators $\hat{J}_{\mu,\nu} = \sum_{i=1}^N (|\mu\rangle\langle\nu|)_i$ (N is the number of atoms) obeying

$$[\hat{J}_{\mu,\nu}, \hat{J}_{\nu',\mu'}] = \delta_{\nu,\nu'} \hat{J}_{\mu,\mu'} - \delta_{\mu,\mu'} \hat{J}_{\nu,\nu'} \quad (2)$$

and g is the atom-cavity coupling strength. \hat{a} and \hat{a}^\dagger are the annihilation and creation operators for the cavity photons, respectively. The coupling constant β is proportional to the second-order susceptibility tensor of the nonlinear crystal and to the amplitude of the external pump field [19]. Here we assume the far-detuned atom-light field and atom-cavity interactions, $|\Delta_{c,p}| \gg \Omega, g$. Hence, we can ignore the effects of atoms inelastically scattering photons (the atomic spontaneous emission) on the atom-cavity dynamics [22,23]. The strength β is adjusted to be comparable with the detunings $\Delta_{c,p}$. Here we assume both frequencies of the driving field and the cavity mode are in the blue-detuned side of their corresponding atomic transitions, respectively, i.e., $\Delta_{c,p} < 0$.

By eliminating the upper state $|3\rangle$ via the Schrieffer-Wolff transformation [24] and expanding to second order in terms of $\frac{\Omega}{\Delta_c}$ and $\frac{g}{\Delta_p}$, the effective Hamiltonian describing the collective

atom-cavity interaction is given by

$$\begin{aligned} \hat{H}/\hbar \approx & \left(\Delta_c + \frac{\Omega^2}{\Delta_c} \right) \hat{J}_{1,1} + \beta(\hat{a}^\dagger \hat{a}^\dagger + \hat{a} \hat{a}) \\ & + \left[\Delta_p + \frac{g^2}{\Delta_p} \hat{a}^\dagger \hat{a} - \frac{\beta g^2}{\Delta_p^2} (\hat{a}^\dagger \hat{a}^\dagger + \hat{a} \hat{a}) \right] \hat{J}_{2,2} \\ & + g_R \left(\hat{a}^\dagger - \frac{2\beta}{\Delta_c + \Delta_p} \hat{a} \right) \frac{\hat{J}_-}{\sqrt{N}} \\ & + g_R \left(\hat{a} - \frac{2\beta}{\Delta_c + \Delta_p} \hat{a}^\dagger \right) \frac{\hat{J}_+}{\sqrt{N}}, \end{aligned} \quad (3)$$

where we have defined the collective Raman-transition strength [16]

$$g_R = \frac{\sqrt{N} g \Omega}{2 \Delta_c \Delta_p} (\Delta_c + \Delta_p) \quad (4)$$

and the collective spin operators $\hat{J}_- = \sum_i (|2\rangle\langle 1|)_i$ and $\hat{J}_+ = \sum_i (|1\rangle\langle 2|)_i$. Note that the atom-light field interaction causes a light shift $\frac{\Omega^2}{\Delta_c}$ to the atomic $|1\rangle$ state while the atom-cavity coupling and the parametric amplification process induce extra ac Stark shifts $\frac{g^2}{\Delta_p} \hat{a}^\dagger \hat{a}$ and $-\frac{\beta g^2}{\Delta_p^2} (\hat{a}^\dagger \hat{a}^\dagger + \hat{a} \hat{a})$ to $|2\rangle$. The relative energy splitting Δ_R between the $|1\rangle$ and $|2\rangle$ states,

$$\begin{aligned} \Delta_R = & \delta_R + \frac{g^2}{4\Delta_p} \left(\frac{2\beta}{\Delta_p} - 1 \right) (\hat{a}^\dagger + \hat{a})^2 \\ & - \frac{g^2}{4\Delta_p} \left(\frac{2\beta}{\Delta_p} + 1 \right) [i(\hat{a}^\dagger - \hat{a})]^2, \end{aligned} \quad (5)$$

can be enlarged or reduced by choosing the sign of β . Here we have defined the Raman detuning

$$\delta_R = \Delta_c - \Delta_p + \frac{\Omega^2}{\Delta_c} + \frac{g^2}{2\Delta_p}, \quad (6)$$

which includes the ac Stark shifts induced by the atom-light field and atom-single photon interactions. Moreover, the collective counter-rotating terms $(\hat{a} \hat{J}_-, \hat{a}^\dagger \hat{J}_+)$, which are particularly important in the common Dicke model [1], are presented in Hamiltonian (3) due to the nonlinear parametric oscillation modulating the collective atom-cavity dynamics. In addition, the relative strengths between the collective counter-rotating terms $(\hat{a} \hat{J}_-, \hat{a}^\dagger \hat{J}_+)$ and the collective rotating terms $(\hat{a}^\dagger \hat{J}_-, \hat{a} \hat{J}_+)$ can be adjusted by changing the coupling constant β and the atom-light and atom-cavity detunings $\Delta_{c,p}$ in experiment. In the following, we assume $\beta < 0$ and one can apply the same approach to analyze other cases.

There are three terms in Hamiltonian (3) that lead to generation of photons in the cavity: (i) The $g_R \hat{a}^\dagger \hat{J}_-$ term denotes one atom in the $|1\rangle$ state (spin up) transiting to the $|2\rangle$ state (spin down) via a coherent Raman process with a rate of g_R . (ii) The parametric down-conversion denoted by $\beta \hat{a}^\dagger \hat{a}^\dagger$ produces a pair of intracavity photons at a rate of β . (iii) The term $g_R \frac{2\beta}{\Delta_c + \Delta_p} \hat{a}^\dagger \hat{J}_+$, also due to the parametric down-conversion, indicates one atom in the $|2\rangle$ state transits to the $|1\rangle$ state via absorbing one of two generated photons with the other photon being left inside the cavity. Hamiltonian evolution must be reversible. Thus, there are also conjugate terms to

processes (i)–(iii), which result in the annihilation of photons in the cavity but through the exchange mechanism. We should note that processes (ii) and (iii) strongly depend on each other as they are both a function of β . When $|\beta| > \frac{1}{2} |\Delta_c + \Delta_p|$, processes (ii) and (iii) tend to dominate over process (i). Thus, in this limit, the primary contribution to excitation in the cavity is due to the parametric down-conversion.

B. Superradiant phase transition in a nondissipative system

We now demonstrate that this composite system can display a superradiant phase transition by examining the ground state of a mean-field description of the system when there is no loss of photons from the cavity. We investigate the dependence of the ground state and excitation spectrum of the system on different experimentally adjustable parameters. We write Hamiltonian (3) in the compact form (the spin-boson model)

$$\begin{aligned} \hat{H}/\hbar = & \delta_R \hat{J}_z + \Delta_p \left(\frac{\beta}{2\Delta_p} + \frac{\mu(\beta) \hat{J}_z}{4N} \right) (\hat{a}^\dagger + \hat{a})^2 \\ & + \Delta_p \left(\frac{-\beta}{2\Delta_p} + \frac{\mu(-\beta) \hat{J}_z}{4N} \right) [i(\hat{a}^\dagger - \hat{a})]^2 \\ & + \Delta_p \frac{\nu(\beta)}{2} (\hat{a}^\dagger + \hat{a}) \frac{\hat{J}_+ + \hat{J}_-}{\sqrt{N}} \\ & + \Delta_p \frac{\nu(-\beta)}{2} [i(\hat{a}^\dagger - \hat{a})] \frac{i(\hat{J}_+ - \hat{J}_-)}{\sqrt{N}}, \end{aligned} \quad (7)$$

where $\hat{J}_z = \frac{1}{2} (\hat{J}_{1,1} - \hat{J}_{2,2})$ is the z component of the total pseudospin of length $\frac{N}{2}$. One can confirm the angular momentum commutation relations

$$[\hat{J}_+, \hat{J}_-] = 2\hat{J}_z, \quad [\hat{J}_\pm, \hat{J}_z] = \mp \hat{J}_\pm.$$

The function $\mu(\pm\beta) = \frac{Ng^2}{\Delta_p^2} (\pm \frac{2\beta}{\Delta_p} - 1)$, which is proportional to the atomic number N , is related to the extra light shift induced by the optical parametric process [see Eq. (5)], while the function $\nu(\pm\beta) = \frac{g_R}{\Delta_p} (1 \mp \frac{2\beta}{\Delta_c + \Delta_p})$ scaled with \sqrt{N} denotes the strength of the Raman transition between $|1\rangle$ and $|2\rangle$. Increasing the system size N adjusts the light shifts and enhances the collective atom-cavity interaction.

1. Ground state

In order to determine the ground state of the atom-cavity system, we transform the Hamiltonian \hat{H} into the Holstein-Primakoff representation [25]. We make the following replacements:

$$\begin{aligned} \hat{J}_- = & \sqrt{N - \hat{b}^\dagger \hat{b}} \hat{b}, \quad \hat{J}_+ = \hat{b}^\dagger \sqrt{N - \hat{b}^\dagger \hat{b}}, \\ \hat{J}_z = & \hat{b}^\dagger \hat{b} - N/2, \end{aligned}$$

where \hat{b} and \hat{b}^\dagger satisfy the bosonic commutation relation $[\hat{b}, \hat{b}^\dagger] = 1$ and $0 \leq \hat{b}^\dagger \hat{b} \leq N$.

We also introduce two macroscopic displacements to both bosonic modes \hat{a} and \hat{b} . The displacement operators $\hat{D}(\sqrt{N}A) = e^{\sqrt{N}(A\hat{a}^\dagger - A^*\hat{a})}$ and $\hat{D}(\sqrt{N}B) = e^{\sqrt{N}(B\hat{b}^\dagger - B^*\hat{b})}$ are

applied to the Hamiltonian as follows:

$$\hat{\mathcal{H}} = \hat{D}^\dagger(\sqrt{N}B)\hat{D}^\dagger(\sqrt{N}A)\hat{H}\hat{D}(\sqrt{N}A)\hat{D}(\sqrt{N}B). \quad (8)$$

Finally, in the limit of the large atomic number (here we assume reasonably that N is larger than 10^2) the displaced Hamiltonian $\hat{\mathcal{H}}$ can be approximated by the expansion to second order in the boson operators [26], e.g.,

$$\begin{aligned} & \sqrt{N - (\hat{b}^\dagger + \sqrt{N}B^*)(\hat{b} + \sqrt{N}B)} \\ & \approx \sqrt{N(1 - B^*B)} \left[1 - \frac{\hat{b}^\dagger \hat{b}}{2N(1 - B^*B)} \right. \\ & \quad \left. - \frac{(B^*\hat{b} + B\hat{b}^\dagger)}{2\sqrt{N}(1 - B^*B)} - \frac{(B^*\hat{b} + B\hat{b}^\dagger)^2}{8N(1 - B^*B)^2} \right], \quad (9) \end{aligned}$$

and one obtains $\hat{\mathcal{H}} \approx \mathcal{E}_0 + \hat{\mathcal{H}}_1 + \hat{\mathcal{H}}_2$, where

$$\begin{aligned} \mathcal{E}_0/(N\hbar) &= \delta_R n_b + 2\beta(X_A^2 - Y_A^2) \\ & \quad + 2\Delta_p [\nu(\beta)X_A X_B + \nu(-\beta)Y_A Y_B] \sqrt{1 - n_b} \\ & \quad + \Delta_p [\mu(\beta)X_A^2 - \mu(-\beta)Y_A^2] (n_b - 1/2) \quad (10) \end{aligned}$$

is the classical ground-state energy. $\hat{\mathcal{H}}_1$ and $\hat{\mathcal{H}}_2$ are linear and quadratic with regard to bosonic operators, respectively. Here we have defined $X_A = (A^* + A)/2$, $Y_A = i(A^* - A)/2$, $X_B = (B^* + B)/2$, $Y_B = i(B^* - B)/2$, and the mean-field photon and excited-atom numbers $n_a \equiv A^*A = X_A^2 + Y_A^2$ and $n_b \equiv B^*B = X_B^2 + Y_B^2$.

We can find the mean-field solution to our system by choosing variables A and B such that the linear displacement Hamiltonian $\hat{\mathcal{H}}_1 = 0$. Using this technique, we find A and B must satisfy

$$\begin{aligned} & \frac{\delta_R}{\Delta_p} X_B + [\mu(\beta)X_A^2 + \mu(-\beta)Y_A^2]X_B - \nu(-\beta) \frac{X_B Y_A Y_B}{\sqrt{1 - n_b}} \\ & \quad + \nu(\beta)X_A \left(\sqrt{1 - n_b} - \frac{X_B^2}{\sqrt{1 - n_b}} \right) = 0, \quad (11) \end{aligned}$$

$$\begin{aligned} & \frac{\delta_R}{\Delta_p} Y_B + [\mu(\beta)X_A^2 + \mu(-\beta)Y_A^2]Y_B - \nu(\beta) \frac{X_A X_B Y_B}{\sqrt{1 - n_b}} \\ & \quad + \nu(-\beta)Y_A \left(\sqrt{1 - n_b} - \frac{Y_B^2}{\sqrt{1 - n_b}} \right) = 0, \quad (12) \end{aligned}$$

$$\left[\frac{2\beta}{\Delta_p} - \frac{\mu(\beta)}{2} (1 - 2n_b) \right] \frac{X_A}{X_B} + \nu(\beta)\sqrt{1 - n_b} = 0, \quad (13)$$

$$\left[\frac{2\beta}{\Delta_p} + \frac{\mu(-\beta)}{2} (1 - 2n_b) \right] \frac{Y_A}{Y_B} - \nu(-\beta)\sqrt{1 - n_b} = 0. \quad (14)$$

It is easy to verify the trivial solution $\mathcal{E}_0 = A = B = 0$, which denotes all atoms are in the spin-down state $|2\rangle$ and no photons exist inside the cavity, always satisfies Eqs. (12)–(14). We call this trivial solution the “normal” phase of the quantum system, as there is no macroscopic occupation of either bosonic mode.

By solving Eqs. (12)–(14) we obtain the nontrivial ground-state solution,

$$X_A = X_B = 0, \quad (15)$$

$$n_b = \frac{W_-}{\mu(-\beta)} \left[1 - \sqrt{1 - \frac{\mu(-\beta)}{W_-} \left(1 - \frac{\delta_R}{\Delta_p} \frac{W_+}{Q} \right)} \right], \quad (16)$$

$$n_a = \frac{\nu^2(-\beta)}{[W_- + \mu(-\beta)n_b]^2} n_b (1 - n_b), \quad (17)$$

and the ground-state energy,

$$\begin{aligned} \mathcal{E}_0/(N\hbar) &= \delta_R n_b - 2\beta Y_A^2 + 2\Delta_p \nu(-\beta) Y_A Y_B \sqrt{1 - n_b} \\ & \quad - \Delta_p \mu(-\beta) Y_A^2 (n_b - 1/2), \quad (18) \end{aligned}$$

where $W_\pm = \frac{\mu(-\beta)}{2} \pm \frac{-2\beta}{\Delta_p}$ and $Q = \nu^2(-\beta) + \frac{\delta_R}{\Delta_p} \mu(-\beta)$. We find that when $\frac{\delta_R}{\Delta_p} > 0$ (the negative Raman detuning) and $Q > W_+$ the average population n_b is real and $0 < n_b \leq 1$ and furthermore the ground energy \mathcal{E}_0 becomes negative, which means a phase transition occurs in the atom-cavity system. Neither Ω nor g can be adjusted over a wide range given a fixed pair of $\Delta_{c,p}$, as we have assumed the far-detuned atom-light field and atom-cavity interactions. Instead, here we adjust the collective atom-cavity interaction by changing the system size N .

Figure 2(a) displays the average mean-field occupations $n_{a,b}$ as a function of the system size N , where the system is in the normal state $n_{a,b} = 0$ for the atomic number N smaller than a critical value N_c while $n_{a,b} \neq 0$ for $N > N_c$. Meanwhile, the corresponding energy of the ground state \mathcal{E}_0 becomes negative [see Fig. 2(b)], which denotes the quantum system transiting to a new phase, i.e., the superradiant phase. By examining the derivatives of \mathcal{E}_0 around N_c , we find that the first derivative is continuous [see Fig. 2(c)] while the second derivative possesses a discontinuity at N_c [see Fig. 2(d)], which indicates a second-order phase transition.

For a small number of atoms, the relatively large Raman detuning $\delta_R \neq 0$ suppresses the coherent Raman transition from $|2\rangle$ to $|1\rangle$, which provides a high threshold for the degenerate parametric oscillation. Thus, all atoms are in the spin-down state ($|2\rangle$) and no photons exist inside cavity. As N is increased, the collective Raman transition strength ($\propto g_R = \sqrt{N}\Omega g \frac{(\Delta_p + \Delta_c)}{\Delta_p \Delta_c}$) is dramatically enhanced and overcomes the suppression of nonzero Raman detuning when $N > N_c$. Consequently, a coherent atom-cavity dynamics is established and $n_{a,b} > 0$. In order to maintain the collective Raman transition between $|1\rangle$ and $|2\rangle$, an intense intracavity field is required around the critical point.

When N is further increased, the behavior of the intercavity field is different from that in the usual Dicke model [1], i.e., n_a goes down while n_b is gradually saturated as shown in Fig. 2. We make the following three observations to explain why this is the case. (i) As more atoms are populated in the $|1\rangle$ state the Raman transition from $|2\rangle$ to $|1\rangle$ is reduced, which ceases the amplification of the intracavity field. (ii) The larger N further amplifies the atom-cavity coupling, which means the collective Raman transition can be maintained without necessarily needing a strong intracavity field. (iii) In Eq. (17)

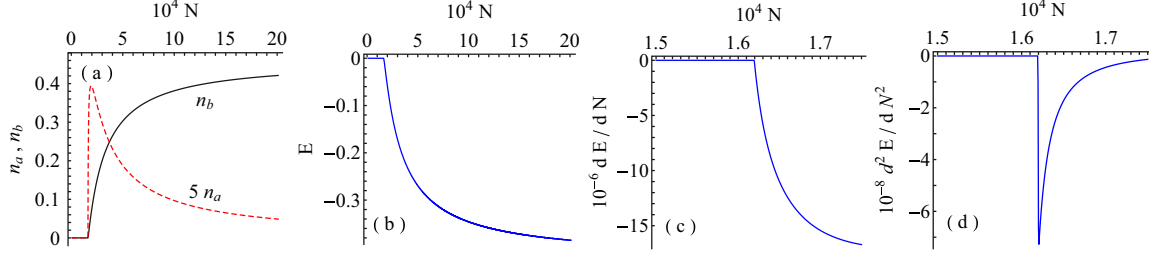


FIG. 2. (Color online) (a) n_b (solid line) and n_a (dashed line) as a function of the system size N with $\Omega = 10g$, $\Delta_c = -200g$, $\Delta_p = -100g$, and $\beta = 2\Delta_p$. (b) The corresponding ground-state energy \mathcal{E}_0 . When N is larger than the critical atomic number $N_c = 1.62 \times 10^4$, \mathcal{E}_0 becomes negative. The first and second derivatives of the ground-state energy with respect to N around N_c are displayed in panels (c) and (d), respectively. Here we have defined $E \equiv \frac{\mathcal{E}_0}{N\hbar|\Delta_p|}$.

the numerator is proportional to N while the denominator scales with N^2 . Therefore, further enlarging the system size results in the decrease of the intracavity photons n_a .

Besides N , the intracavity field strongly depends on the Raman detuning δ_R . As shown in Figs. 3(a) and 3(b), making δ_R more negative dramatically increases the occupation of cavity mode, especially around the critical point, though δ_R rarely affects n_b . For a system in the superradiant phase, more intracavity photons are required to overcome the suppression of the collective Raman transition from the larger negative δ_R . Moreover, around the critical system size N_c the number of intracavity photons n_a can much exceed that of atoms in the spin-up state n_b by increasing δ_R more negatively.

From Eq. (17) one finds that the critical number N_c of atoms is determined by the following equation

$$\frac{\delta_R}{\Delta_p} \left[\frac{2\beta}{\Delta_p} + \frac{\mu(-\beta)}{2} \right] + v^2(-\beta) = 0. \quad (19)$$

Figure 3(c) displays the dependence of N_c on the Raman detuning δ_R and the coupling strength β . For a fixed β , N_c can be only affected by a small δ_R around the resonance Raman transition. For a large negative δ_R , Eq. (19) can be approximately simplified as

$$N_c \approx \frac{2\Delta_p^2}{g^2} \frac{2\beta}{2\beta + \Delta_p}. \quad (20)$$

Reducing $|\Delta_p|$ and enlarging g as much as possible can be used to reduce N_c . Another option is to make $|\beta|$ smaller than $|\Delta_p|$. However, the derivation for our effective Hamiltonian (3) breaks down as we previously assumed that $|\beta|$ is the same order or larger than $|\Delta_p|$.

2. Excitation spectrum

We have recognized a second-order phase transition in our mean-field analysis. The next logical question to ask is the following: What continuous symmetry in our system is spontaneously broken? We can determine this by looking at the low-excitation spectrum of the system. One can find this spectrum by diagonalizing the bilinear Hamiltonian $\hat{\mathcal{H}}_2$, which can be expressed in a general form,

$$\begin{aligned} \hat{\mathcal{H}}_2/\hbar = & u_+(\hat{a}^\dagger + \hat{a})^2 + v_+(\hat{b}^\dagger + \hat{b})^2 + u_-[i(\hat{a}^\dagger - \hat{a})]^2 \\ & + v_-[i(\hat{b}^\dagger - \hat{b})]^2 + \lambda_+(\hat{a}^\dagger + \hat{a})(\hat{b}^\dagger + \hat{b}) \\ & + \lambda_-[i(\hat{a}^\dagger - \hat{a})][i(\hat{b}^\dagger - \hat{b})], \end{aligned} \quad (21)$$

where for brevity we have defined $u_+ = \frac{\Delta_p}{4} \left[\frac{2\beta}{\Delta_p} - \frac{\mu(-\beta)}{2}(1 - 2n_b) \right]$, $u_- = \frac{\Delta_p}{4} \left[-\frac{2\beta}{\Delta_p} - \frac{\mu(-\beta)}{2}(1 - 2n_b) \right]$, $v_+ = \frac{\Delta_p}{4} \left[\frac{\delta_R}{\Delta_p} + \mu(-\beta)n_a - v(-\beta) \frac{Y_A Y_B}{\sqrt{1-n_b}} \right]$, $v_- = \frac{\Delta_p}{4} \left[\frac{\delta_R}{\Delta_p} + \mu(-\beta)n_a - v(-\beta) \frac{(3-2n_b)Y_A Y_B}{(1-n_b)^{3/2}} \right]$, $\lambda_+ = \frac{\Delta_p}{2} v(\beta)\sqrt{1-n_b}$, and $\lambda_- = \Delta_p \left[\mu(-\beta)Y_A Y_B + \frac{v(-\beta)}{2} \frac{1-2n_b}{\sqrt{1-n_b}} \right]$.

Following the same approach in Ref. [27], one finds the following Bogoliubov transformation for the new bosonic operators $\hat{e}_{a,p}$,

$$\hat{e}_{a,p} = h_1 \hat{a}^\dagger + h_2 \hat{a} + h_3 \hat{b}^\dagger + h_4 \hat{b}, \quad (22)$$

where the parameters are defined as

$$\begin{aligned} h_1 = & \left(\sqrt{\frac{\epsilon_{a,p}}{8u_-}} f_- - \sqrt{\frac{2u_-}{\epsilon_{a,p}}} \frac{1}{f_-} \right) \cos \phi \\ & + \left(-\sqrt{\frac{\epsilon_{a,p}}{8u_-}} f_+ + \sqrt{\frac{2u_-}{\epsilon_{a,p}}} \frac{1}{f_+} \right) \sin \phi, \end{aligned} \quad (23)$$

$$\begin{aligned} h_2 = & \left(\sqrt{\frac{\epsilon_{a,p}}{8u_-}} f_- + \sqrt{\frac{2u_-}{\epsilon_{a,p}}} \frac{1}{f_-} \right) \cos \phi \\ & + \left(-\sqrt{\frac{\epsilon_{a,p}}{8u_-}} f_+ - \sqrt{\frac{2u_-}{\epsilon_{a,p}}} \frac{1}{f_+} \right) \sin \phi, \end{aligned} \quad (24)$$

$$\begin{aligned} h_3 = & \left(-\sqrt{\frac{\epsilon_{a,p}}{8v_-}} f_- + \sqrt{\frac{2v_-}{\epsilon_{a,p}}} \frac{1}{f_-} \right) \cos \phi \\ & + \left(-\sqrt{\frac{\epsilon_{a,p}}{8v_-}} f_+ + \sqrt{\frac{2v_-}{\epsilon_{a,p}}} \frac{1}{f_+} \right) \sin \phi, \end{aligned} \quad (25)$$

$$\begin{aligned} h_4 = & \left(-\sqrt{\frac{\epsilon_{a,p}}{8v_-}} f_- - \sqrt{\frac{2v_-}{\epsilon_{a,p}}} \frac{1}{f_-} \right) \cos \phi \\ & + \left(-\sqrt{\frac{\epsilon_{a,p}}{8v_-}} f_+ - \sqrt{\frac{2v_-}{\epsilon_{a,p}}} \frac{1}{f_+} \right) \sin \phi, \end{aligned} \quad (26)$$

and the excitation energies of two independent oscillator modes are given by

$$\epsilon_{a,p} = (U + V) \pm \sqrt{(U - V)^2 + L^2}, \quad (27)$$

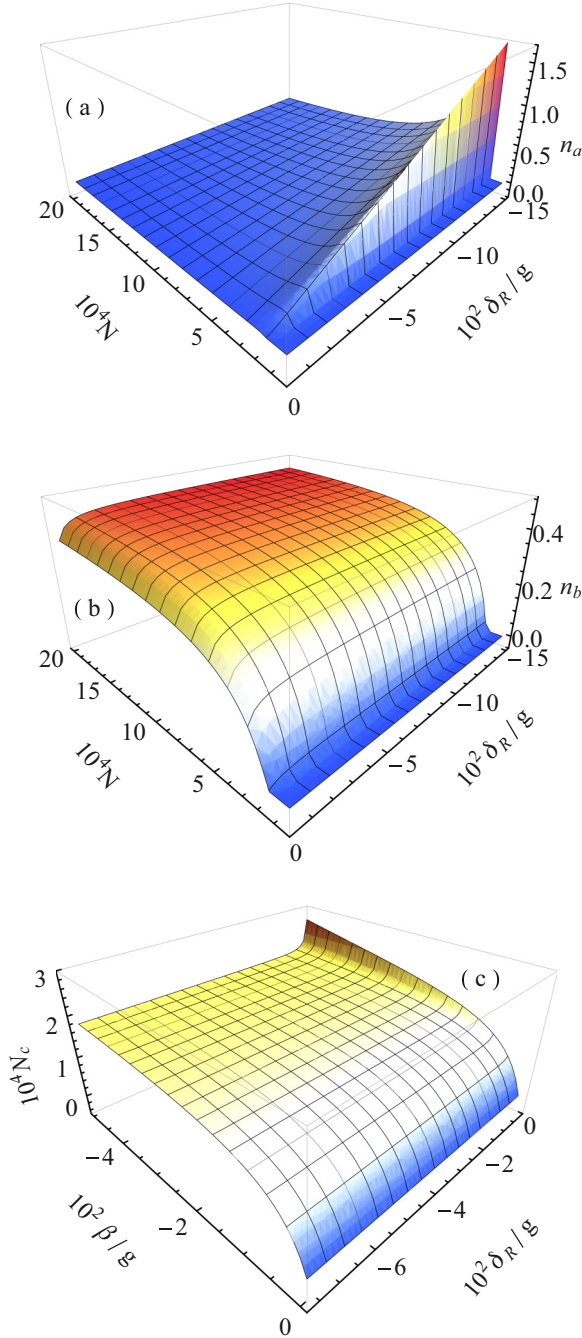


FIG. 3. (Color online) (a) and (b): The average numbers of two kinds of bosons, i.e., n_a and n_b , as a function of the number N of atoms and the Raman detuning δ_R with $\beta = 2\Delta_p$. (c) The critical atomic number N_c as a function of the strength β of the parametric down-conversion and different Raman detuning δ_R . For all figures, $\Omega = 10g$ and $\Delta_p = -100g$. δ_R is adjusted by changing the detuning Δ_c .

where we have written $U = \frac{4}{f_+^2}(u_+u_- + v_+v_- - \lambda_+\sqrt{u_-v_-})$, $V = \frac{4}{f_+^2}(u_+u_- + v_+v_- + \lambda_+\sqrt{u_-v_-})$, $L = \frac{8}{f_+f_-}(u_+u_- - v_+v_-)$, $\tan\phi = -\frac{L}{U-V}$, and $f_{\pm} = (\frac{1}{2} \pm \frac{\lambda_{\pm}}{2\sqrt{u_-v_-}})^{-1/2}$. The bilinear Hamiltonian $\hat{\mathcal{H}}_2$ is finally expressed as

$$\hat{\mathcal{H}}_2/\hbar = \epsilon_a \hat{e}_a^\dagger \hat{e}_a + \epsilon_p \hat{e}_p^\dagger \hat{e}_p. \quad (28)$$

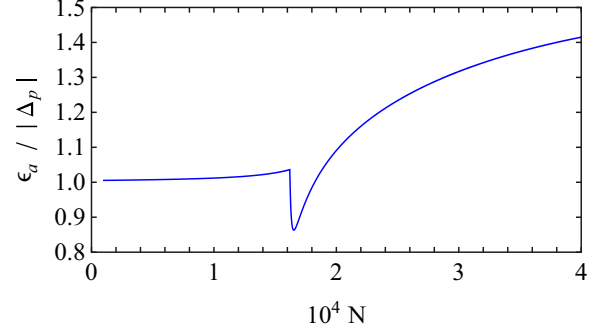


FIG. 4. (Color online) Excitation energy ϵ_a corresponding to Fig. 2 as a function of the system size N .

Figure 4 displays the numerical results of excitation energies. When $N < N_c$ only the ‘‘atomic’’ branch ϵ_a , which starts from $|\delta_R|$, is valid, while ϵ_p is an imaginary number. This is because in the normal state $A = B = 0$ the quadratic term $\beta(\hat{a}^\dagger \hat{a}^\dagger + \hat{a} \hat{a})$ in Hamiltonian (3) cannot be diagonalized via the Bogoliubov transformation, which leads to the absence of the ‘‘photonic’’ branch ϵ_p . After the critical point $N > N_c$, ϵ_a goes up rapidly and ϵ_p is still invalid.

The global parity operator associated with Hamiltonian (7) is given by $\hat{\Pi} = \exp(i\pi \hat{\Xi})$, where

$$\hat{\Xi} = \hat{a}^\dagger \hat{a} + \hat{J}_z + N \quad (29)$$

counts the total number of excitation quanta [28], and it is easy to verify the commutation relation

$$[\hat{H}, \hat{\Pi}] = 0, \quad (30)$$

which means a conserved parity. In the Holstein-Primakoff representation the parity operator $\hat{\Pi}$ becomes

$$\hat{\Pi} = \exp[i\pi(\hat{a}^\dagger \hat{a} + \hat{b}^\dagger \hat{b})]. \quad (31)$$

After doing the replacements $\hat{a} \rightarrow A + \hat{a}$ and $\hat{b} \rightarrow B + \hat{b}$ we obtain

$$\hat{\Pi} = \exp[i\pi(\hat{a}^\dagger \hat{a} + \hat{b}^\dagger \hat{b} + A\hat{a}^\dagger + A^*\hat{a} + B\hat{b}^\dagger + B^*\hat{b} + Nn_a + Nn_b)].$$

In the normal state $n_a = n_b = 0$, $\hat{\mathcal{H}}_2$ is reduced back to Hamiltonian (7), for which the global parity is conserved. However, when $N > N_c$, $\hat{\mathcal{H}}_2$ does not commute with $\hat{\Pi}$ due to $A \neq 0$ and $B \neq 0$, which denotes the symmetry of the ground state becomes spontaneously broken at N_c [10]. For the Dicke superradiant phase, one can define the local parity operator as

$$\hat{\Pi}_2 = \exp[i\pi(\hat{e}_a^\dagger \hat{e}_a + \hat{e}_p^\dagger \hat{e}_p)], \quad (32)$$

which obviously commutes with $\hat{\mathcal{H}}_2$.

C. Dissipative atom-cavity system

So far, we have only discussed an ideal atom-cavity system without any dissipation. However, the energy loss due to the atomic spontaneous emission and cavity loss occurs on a time scale that is relevant to the coherent dynamics in real experiments. Thus, studying the influence of the dissipation on the system dynamics is essential.

In our system, the inelastic photon scattering (the spontaneous emission of atoms) rarely contributes to the energy loss due to the far-detuned atom-light field and atom-cavity interactions [15]. Here we consider the relatively larger dissipative mechanism, the cavity loss, by employing the quantum Langevin method [29]. Following the same approach in Refs. [30–33], the Heisenberg-Langevin equations for the photon and collective atomic operators are written as

$$\begin{aligned} \frac{d}{dt}\hat{x}_a(t) &= -\frac{\kappa}{2}\hat{x}_a(t) + \Delta_p \left[-\frac{2\beta}{\Delta_p} + \mu(-\beta)\hat{j}_z(t) \right] \hat{y}_a(t) \\ &\quad - \Delta_p \nu(-\beta)\hat{j}_y(t) + \hat{f}_{\kappa,x}(t), \end{aligned} \quad (33)$$

$$\begin{aligned} \frac{d}{dt}\hat{y}_a(t) &= -\frac{\kappa}{2}\hat{y}_a(t) - \Delta_p \left[\frac{2\beta}{\Delta_p} + \mu(\beta)\hat{j}_z(t) \right] \hat{x}_a(t) \\ &\quad - \Delta_p \nu(-\beta)\hat{j}_x(t) + \hat{f}_{\kappa,y}(t), \end{aligned} \quad (34)$$

$$\begin{aligned} \frac{d}{dt}\hat{j}_x(t) &= -\delta_R\hat{j}_y(t) - \Delta_p [\mu(\beta)\hat{x}_a^2(t) + \mu(-\beta)\hat{y}_a^2(t)]\hat{j}_y(t) \\ &\quad - 2\Delta_p \nu(-\beta)\hat{y}_a(t)\hat{j}_z(t), \end{aligned} \quad (35)$$

$$\begin{aligned} \frac{d}{dt}\hat{j}_y(t) &= \delta_R\hat{j}_x(t) + \Delta_p [\mu(\beta)\hat{x}_a^2(t) + \mu(-\beta)\hat{y}_a^2(t)]\hat{j}_x(t) \\ &\quad - 2\Delta_p \nu(\beta)\hat{x}_a(t)\hat{j}_z(t), \end{aligned} \quad (36)$$

$$\frac{d}{dt}\hat{j}_z(t) = 2\Delta_p \nu(\beta)\hat{x}_a(t)\hat{j}_y(t) + 2\Delta_p \nu(-\beta)\hat{y}_a(t)\hat{j}_x(t), \quad (37)$$

where we have defined the operator variables

$$\begin{aligned} \hat{x}_a(t) &\equiv \frac{[\hat{a}^+(t) + \hat{a}(t)]}{2\sqrt{N}}, & \hat{y}_a(t) &\equiv \frac{i[\hat{a}^+(t) - \hat{a}(t)]}{2\sqrt{N}}, \\ \hat{j}_x(t) &\equiv \frac{[\hat{J}_+(t) + \hat{J}_-(t)]}{2N}, & \hat{j}_y(t) &\equiv \frac{i[\hat{J}_+(t) - \hat{J}_-(t)]}{2N}, \\ \hat{j}_z(t) &\equiv \frac{\hat{J}_z(t)}{N}. \end{aligned}$$

κ is the loss rate of intracavity photons. The operators

$$\hat{f}_{\kappa,x}(t) = \frac{[\hat{f}^\dagger(t) + \hat{f}(t)]}{2\sqrt{N}} \quad \text{and} \quad \hat{f}_{\kappa,y}(t) = \frac{i[\hat{f}^\dagger(t) - \hat{f}(t)]}{2\sqrt{N}}$$

describe the quantum noises injected at the cavity output mirror. The Langevin noise force $\hat{f}(t)$ satisfies the commutation relation

$$[\hat{f}(t), \hat{f}^\dagger(t')] = \kappa \delta(t - t') \quad (38)$$

and correlation functions [31]

$$\begin{aligned} \langle \hat{f}(t) \rangle &= \langle \hat{f}^\dagger(t) \rangle = \langle \hat{f}^\dagger(t)\hat{f}(t') \rangle = 0, \\ \langle \hat{f}(t)\hat{f}^\dagger(t') \rangle &= \kappa \delta(t - t'), \end{aligned}$$

where we have assumed that the thermal reservoir is at zero temperature. Thus, the mean number of quanta in the thermal reservoir is zero, $n_{\text{th}} = 0$. In addition, according to the input-output theory in Ref. [34], the operators for the cavity output

field are given by

$$\hat{a}_{\text{out}}(t) = \sqrt{\kappa}\hat{a}(t) - \frac{\hat{f}(t)}{\sqrt{\kappa}}, \quad \hat{a}_{\text{out}}^\dagger(t) = \sqrt{\kappa}\hat{a}^\dagger(t) - \frac{\hat{f}^\dagger(t)}{\sqrt{\kappa}},$$

from which one can study the different output-field spectra. Finally, we should note that the above dynamic equations must conserve the pseudoangular momentum

$$\hat{J}_x^2 + \hat{J}_y^2 + \hat{J}_z^2 = \frac{1}{4}. \quad (39)$$

1. Steady-state solution

By taking the quantum average of each operator variable ($O(t) = \langle \hat{O}(t) \rangle$) in the Heisenberg-Langevin equations (34)–(37) and neglecting the quantum fluctuations

$$\langle \hat{O}_1(t)\hat{O}_2(t) \rangle \approx \langle \hat{O}_1(t) \rangle \langle \hat{O}_2(t) \rangle, \quad (40)$$

one can obtain a set of semiclassical equations of motion. For a dissipative system, we are interested in the atom-cavity dynamics on a time scale much longer than the cavity photon lifetime κ^{-1} . In this case, we can set $\frac{d}{dt}O(t) = 0$ and consider the steady-state solutions, which are denoted by the subscript “o”, for example, O_o , of the system. We find the steady states of the composite system by numerically solving the derived semiclassical equations.

Figure 5 displays the average macroscopic occupations of both cavity field ($n_a = x_{a,o}^2 + y_{a,o}^2$) and atomic excitation ($n_b = j_{z,o} + \frac{1}{2}$) changing with the system size N for several different κ . The behaviors of both n_a and n_b are different from those in the normal dissipative Dicke model [15] in the following two aspects: (i) enlarging the cavity loss rate raises the numbers of both intracavity photons and atoms in $|1\rangle$, and (ii) the critical atomic number N_c , at which the superradiant phase transition occurs, moves to a lower value for a larger κ .

Without the cavity loss the intracavity photons can be produced via a combination of degenerate optical parametric oscillation and a coherent Raman transition. After the cavity loss is introduced into the system dynamics, the intracavity photons have a third option, i.e., leaving the resonator through the output mirror. (i) For the system operating in the superradiant phase, more intracavity photons must be generated via the nonlinear optical process so as to maintain the strong collective atom-cavity interaction. This is because a portion of generated photons escape from the optical cavity. In

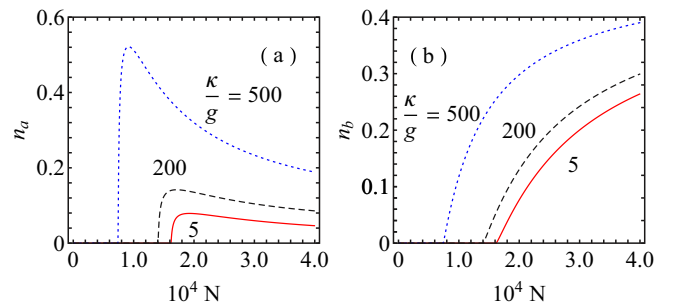


FIG. 5. (Color online) The average numbers of two kinds of bosons n_a and n_b as a function of the number of atoms N for the dissipative atom-cavity system with $\Omega = 10g$, $\Delta_c = -200g$, $\Delta_p = -100g$, and $\beta = 2\Delta_p$.

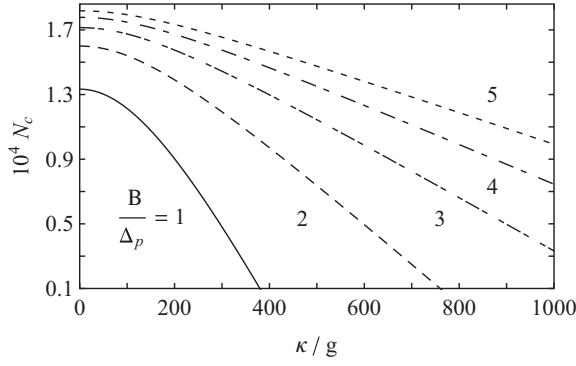


FIG. 6. The critical atomic number N_c as a function of the cavity loss rate κ for several different β . For all curves, $\Omega = 10g$, $\Delta_c = -200g$, and $\Delta_p = -100g$.

return, the more photons profit from the atoms in $|2\rangle$ transiting to $|1\rangle$. As κ is increased, this reciprocal effect is strongly amplified and results in a stronger intracavity field and larger inversion of pseudospins than the case of $\kappa = 0$. (ii) For the composite system in the normal phase, the relative large Raman detuning δ_R suppresses the Raman transition from $|2\rangle$ to $|1\rangle$, thereby impeding the generation of intracavity photons via the degenerate parametric down-conversion. When the cavity loss rate is turned to be large enough, a photon generated via the parametric down-conversion rapidly leaves the cavity without interacting with atoms. Consequently, for a certain atomic number N , at which the nondissipative system stays in the normal phase, a dissipative system may be in the superradiant phase for a large enough κ . Thus, the critical point N_c is reduced as κ is increased.

From Eqs. (34)–(37) we find that N_c can be derived from the following equation:

$$\left(\frac{\kappa/2}{\Delta_p} \frac{\delta_R}{\Delta_p}\right)^2 + \left[\frac{\delta_R}{\Delta_p} \left(\frac{2\beta}{\Delta_p} - \frac{\mu(\beta)}{2}\right) - v^2(\beta)\right] \times \left[\frac{\delta_R}{\Delta_p} \left(-\frac{2\beta}{\Delta_p} - \frac{\mu(-\beta)}{2}\right) - v^2(-\beta)\right] = 0. \quad (41)$$

Figure 6 shows the dependence of N_c on β and κ . For a fixed β , N_c goes down to zero as κ is increased, which means the critical point for the superradiant phase transition vanishes for a large cavity loss rate. However, for $N_c \rightarrow 0$, Eq. (41) is no longer valid since it is derived by neglecting fluctuations in the thermodynamics limit $N \rightarrow \infty$. As N_c approaches zero, the quantum fluctuations dramatically influence the atom-cavity dynamics and its effect cannot be neglected.

2. Stability

We arrive at an important question: Are the steady states derived in the last subsection stable for any system size N ? The stability of a steady state can be analyzed by performing linear stability analysis [35]. First, we consider all the operator variables as the sum of the steady-state solution and a small fluctuating term,

$$\hat{O}(t) = O_o + \delta \hat{O}(t). \quad (42)$$

Based on Eqs. (34)–(37), this results in the following linear differential equations:

$$\begin{aligned} \frac{d}{dt} \delta \hat{x}_a(t) = & -\Delta_p v(-\beta) \delta \hat{j}_y(t) + \Delta_p \mu(-\beta) y_{a,o} \delta \hat{j}_z(t) \\ & + [-2\beta + \Delta_p \mu(-\beta) j_{z,o}] \delta \hat{y}_a(t) \\ & - \frac{\kappa}{2} \delta \hat{x}_a(t) + \hat{f}_{\kappa,x}(t), \end{aligned} \quad (43)$$

$$\begin{aligned} \frac{d}{dt} \delta \hat{y}_a(t) = & -\Delta_p v(\beta) \delta \hat{j}_x(t) - \Delta_p \mu(\beta) x_{a,o} \delta \hat{j}_z(t) \\ & - [2\beta + \Delta_p \mu(\beta) j_{z,o}] \delta \hat{x}_a(t) - \frac{\kappa}{2} \delta \hat{y}_a(t) + \hat{f}_{\kappa,y}(t), \end{aligned} \quad (44)$$

$$\begin{aligned} \frac{d}{dt} \delta \hat{j}_x(t) = & -\Delta_p \left(\frac{\delta_R}{\Delta_p} + \mu(\beta) x_{a,o}^2 + \mu(-\beta) y_{a,o}^2 \right) \delta \hat{j}_y(t) \\ & - 2\Delta_p [\mu(-\beta) j_{y,o} y_{a,o} + v(-\beta) j_{z,o}] \delta \hat{y}_a(t) \\ & - 2\Delta_p \mu(\beta) j_{y,o} x_{a,o} \delta \hat{x}_a(t) - 2\Delta_p v(-\beta) y_{a,o} \delta \hat{j}_z(t), \end{aligned} \quad (45)$$

$$\begin{aligned} \frac{d}{dt} \delta \hat{j}_y(t) = & \Delta_p \left(\frac{\delta_R}{\Delta_p} + \mu(\beta) x_{a,o}^2 + \mu(-\beta) y_{a,o}^2 \right) \delta \hat{j}_x(t) \\ & + 2\Delta_p [\mu(\beta) j_{x,o} x_{a,o} - v(\beta) j_{z,o}] \delta \hat{x}_a(t) \\ & + 2\Delta_p \mu(-\beta) j_{x,o} y_{a,o} \delta \hat{y}_a(t) - 2\Delta_p v(\beta) x_{a,o} \delta \hat{j}_z(t) \end{aligned} \quad (46)$$

$$\begin{aligned} \frac{d}{dt} \delta \hat{j}_z(t) = & 2\Delta_p v(-\beta) y_{a,o} \delta \hat{j}_x(t) + 2\Delta_p v(\beta) x_{a,o} \delta \hat{j}_y(t) \\ & + 2\Delta_p v(\beta) j_{y,o} \delta \hat{x}_a(t) + 2\Delta_p v(-\beta) j_{x,o} \delta \hat{y}_a(t). \end{aligned} \quad (47)$$

By solving the linear differential equations (43)–(47), we can check the steady-state stability and also investigate the quantum fluctuations around them. The fluctuation operators for the output field are expressed as

$$\delta \hat{a}_{\text{out}}(t) = \sqrt{\kappa} \delta \hat{a}(t) - \hat{f}(t)/\sqrt{\kappa}, \quad (48)$$

$$\delta \hat{a}_{\text{out}}^\dagger(t) = \sqrt{\kappa} \delta \hat{a}^\dagger(t) - \hat{f}^\dagger(t)/\sqrt{\kappa}, \quad (49)$$

The noise of the cavity output field originates from the intracavity-field fluctuation and the quantum noise injected at the cavity mirror.

The linear equations (43)–(47) can be written in a matrix form,

$$\frac{d}{dt} \hat{\mathbf{v}}(t) = \mathbf{M} \hat{\mathbf{v}}(t) + \hat{\mathbf{f}}(t), \quad (50)$$

where \mathbf{M} is a constant square matrix and

$$\hat{\mathbf{v}}(t) \equiv (\delta \hat{x}_a(t), \delta \hat{y}_a(t), \delta \hat{j}_x(t), \delta \hat{j}_y(t), \delta \hat{j}_z(t))^T,$$

$$\hat{\mathbf{f}}(t) \equiv (\hat{f}_{\kappa,x}(t), \hat{f}_{\kappa,y}(t), 0, 0, 0)^T.$$

One obtains five eigenvalues by diagonalizing the matrix \mathbf{M} . One of them is always zero because of the interdependence of $\delta \hat{j}_{x,y,z}(t)$, i.e.,

$$j_{x,o} \delta \hat{j}_x(t) + j_{y,o} \delta \hat{j}_y(t) + j_{z,o} \delta \hat{j}_z(t) = 0. \quad (51)$$

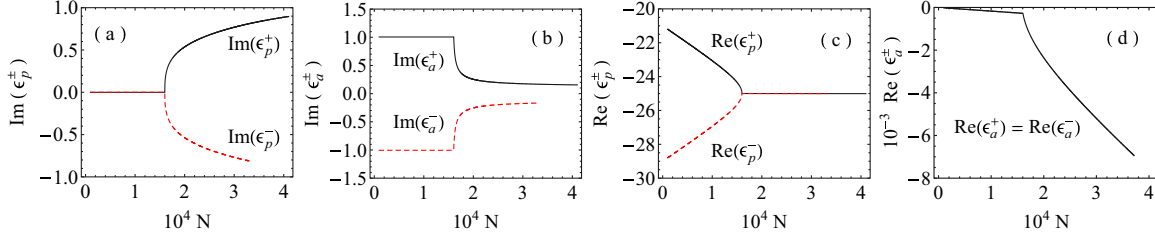


FIG. 7. (Color online) Imaginary and real parts of the atomic (ϵ_a^\pm) and photonic (ϵ_p^\pm) branch eigenvalues (in units of $|\Delta_p|$) as a function of the atomic number N . For all curves, $\Delta_c = -200g$, $\Delta_p = -100g$, $\Omega = 10g$, and $\kappa = 50g$. The critical atomic number for the superradiant phase transition is $N_c \approx 1.61 \times 10^4$.

The other four eigenvalues group into two pairs: one pair ϵ_a^\pm associated with the atomic branch and the other pair ϵ_p^\pm associated with the photonic branch according to the values in the limit of $N \rightarrow 0$. The imaginary parts $\text{Im}(\epsilon_{a,p}^\pm)$ give the different excitation-energy shifts while the real parts $\text{Re}(\epsilon_{a,p}^\pm)$ denote the corresponding damping rates. A stable steady-state solution requires all eigenvalues have negative real parts. It can be checked that when the cavity loss rate κ approaches zero the solution for the dissipative system reduces to the mean-field description of the nondissipative system.

The dependence of two branch eigenvalues on the system size is presented in Fig. 7. For $N < N_c$ the photonic branch eigenvalues have zero imaginary parts $\text{Im}(\epsilon_p^\pm) = 0$ but negative real parts $\text{Re}(\epsilon_p^\pm) < 0$. Due to $\text{Im}(\epsilon_p^\pm) = 0$ there is no photonic excitation in the system. Hence the system is in the normal phase, which is stable. For an initial condition of nonzero photons inside an optical resonator, the intracavity field rapidly decays to zero. In contrast, the atomic branch excitations have a very weak damping rate and nonzero excitation energies $\text{Im}(\epsilon_a^\pm) = \pm|\delta_R|$. For $N > N_c$, the photonic branch excitations are strongly shifted to positive and negative sides, respectively, i.e., $\text{Im}(\epsilon_p^+) > 0$ and $\text{Im}(\epsilon_p^-) < 0$, while both atomic branch excitations approach zero, $\text{Im}(\epsilon_a^\pm) \rightarrow 0$. Moreover, the decay rates of both $\text{Re}(\epsilon_p^\pm)$ are equal to $-\kappa/2$ and $\text{Re}(\epsilon_a^\pm)$ still stay at a very small value. Thus, the energy dissipation of the system in the superradiant phase is primarily from the decay of photonic branch excitations.

3. Spectra of the cavity output field

The light leaking from the cavity can be measured to gain information about the experiment nondestructively [36]. We investigate the influence of the phase transition in the system on the output-field spectra. It is convenient to convert the linear differential equations (43)–(47) from the time domain to the frequency domain via a Fourier transform:

$$\delta \hat{O}(\omega) = \frac{1}{\sqrt{2\pi}} \int_{-\infty}^{\infty} \delta \hat{O}(t) e^{i\omega t} dt, \quad (52)$$

$$\delta \hat{O}^\dagger(-\omega) = \frac{1}{\sqrt{2\pi}} \int_{-\infty}^{\infty} \delta \hat{O}^\dagger(t) e^{-i\omega t} dt. \quad (53)$$

Here, we use the following notation convention: the variable on which a function depends indicates what domain it is in, e.g., $\delta \hat{O}(t)$ indicates the quantum fluctuation in the time domain while $\delta \hat{O}(\omega)$ is in the frequency domain. In addition, the correlation functions associated with the Langevin noise force

$\hat{f}(\omega)$ are given by

$$\begin{aligned} \langle \hat{f}(\omega) \rangle &= \langle \hat{f}^\dagger(\omega) \rangle = \langle \hat{f}^\dagger(-\omega) \hat{f}(\omega') \rangle = 0, \\ \langle \hat{f}(\omega) \hat{f}^\dagger(-\omega') \rangle &= \kappa \delta(\omega + \omega'), \end{aligned}$$

at the zero temperature.

Generally, the normalized spectrum of fluctuations corresponding to an output-field quadrature,

$$\hat{X}_\theta(t) = \frac{1}{2} [\hat{a}_{\text{out}}(t) e^{-i\theta} + \hat{a}_{\text{out}}^\dagger(t) e^{i\theta}], \quad (54)$$

is defined as [31,33]

$$S_\theta(\omega) = \int_{-\infty}^{+\infty} \langle \hat{X}_\theta(t + \tau) \hat{X}_\theta(t) \rangle e^{i\omega\tau} d\tau, \quad (55)$$

where $\langle \hat{X}, \hat{Y} \rangle = \langle \hat{X} \hat{Y} \rangle - \langle \hat{X} \rangle \langle \hat{Y} \rangle$. The spectrum corresponds to a homodyne measurement of the field quadrature component at the angle θ . For $\theta = 0$ we obtain the spectrum of the amplitude fluctuations, while $S_{\theta=\pi/2}(\omega)$ gives us the spectrum of the phase fluctuations of the output field. From Eqs. (48) and (49) we find that $S_\theta(\omega)$ is composed of three parts: the intracavity-field fluctuations, the interaction of field inside the cavity with the vacuum reservoir, and the vacuum fluctuation. In this system the shot-noise limit is $S_\theta(\omega) = \frac{1}{4}$. In Fig. 8, we show two sample spectra for $\theta = 0$ and $\theta = \frac{\pi}{2}$.

For a system size much smaller than N_c , both $S_{\theta=0}(\omega)$ and $S_{\theta=\pi/2}(\omega)$ display a spike doublet associated with the atomic branch eigenvalues ϵ_a^\pm , whose real and imaginary parts determine the widths and positions of two spectral peaks. Additionally, the vacuum noise primarily limits the quadrature spectra at all frequencies except around the atomic branch resonances $\omega \simeq \text{Re}(\epsilon_a^\pm)$, where $S_{\theta=0}(\omega)$ is lower than the shot-noise level while the fluctuations are amplified for $S_{\theta=\pi/2}(\omega)$.

As the system size N approaches N_c , the positions of atomic branch peaks do not change but their widths are broadened. Moreover, another broad peak at $\omega = 0$ appears. This spectral peak grows rapidly and becomes very sharp as $N \rightarrow N_c$. Above the critical point N_c , the height of the central peak decreases dramatically. Thus, the superradiant phase transition is characterized by a divergence of the quadrature spectra at $\omega = 0$. In the same regime, the atomic branch doublet becomes very small and their separation is strongly reduced. Meanwhile, a new pair of peaks associated with the photonic branch eigenvalues ϵ_p^\pm appears as shown in Fig. 7. Last, we note that subshot noise squeezing can be seen in the spectrum. Around $\omega \simeq \text{Re}(\epsilon_p^\pm)$ we find $S_{\theta=0}(\omega)$ becomes squeezed while the conjugate field $S_{\theta=\pi/2}(\omega)$ goes above the shot-noise limit.

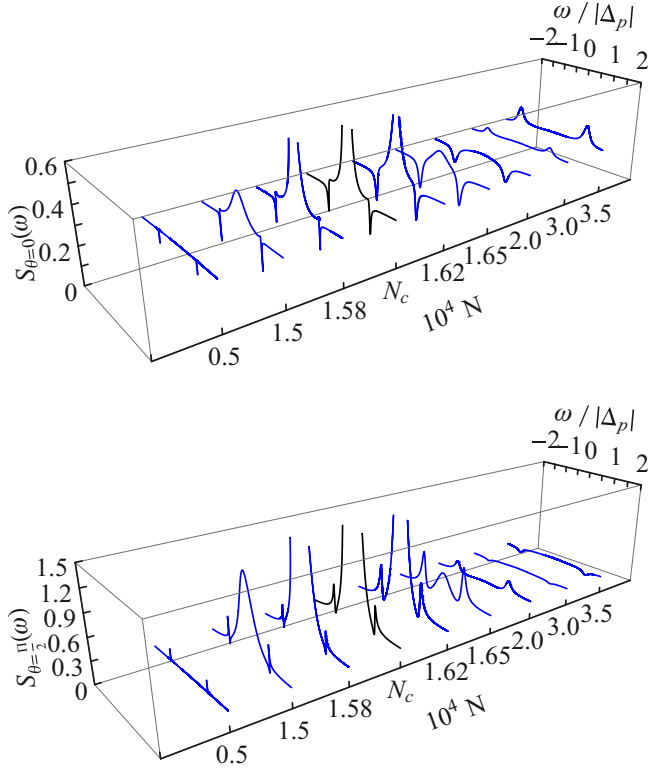


FIG. 8. (Color online) (a) Spectrum of the output-field amplitude fluctuations $S_{\theta=0}(\omega)$ as a function of ω for different system sizes N . The corresponding phase noise spectrum is shown in panel (b). For all curves, the system parameters are the same as those in Fig. 7. The critical atomic number for the superradiant phase transition is $N_c \approx 1.61 \times 10^4$.

Once the system is well above the critical point, the central peak returns to the shot-noise level. $S_{\theta=0}(\omega)$ at the photonic branch resonances changes from having fluctuations that are squeezed to above the shot noise while $S_{\theta=\pi/2}(\omega)$ undergoes the opposite, i.e., from above the shot noise to the squeezed fluctuations. In addition, the separation between two photonic branch peaks continues to increase.

III. LADDER-TYPE ATOMIC SYSTEM

So far, we have discussed the superradiant phase transition in a composite system consisting of a large number of laser-driven three-level Λ -type atoms interacting with a single-mode optical resonator. As discussed in the previous section, the extra intracavity nonlinear parametric oscillation plays an important role in the collective atom-cavity dynamics since it leads to a spin-boson Dicke-like model where the counter-rotating terms of the atom-cavity interactions are presented [see Eq. (7)]. As a consequence, the superradiant phase transition occurs when the system size is larger than a critical value N_c .

In this section, we explore further another type of composite system combined with a degenerate parametric down-conversion process, where an ensemble of ladder-type atoms collectively interact with a single-mode optical resonator. We are motivated by the stronger atom-cavity interaction strength

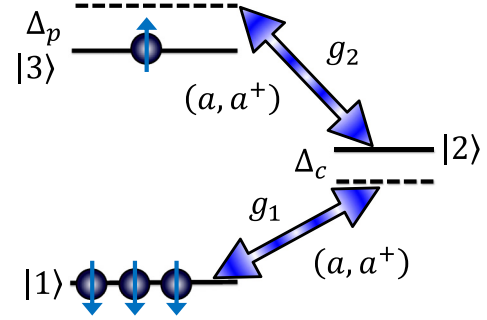


FIG. 9. (Color online) The level structure of three-level ladder-type atom. The single-cavity mode denoted by the photon annihilation and creation operators $(\hat{a}, \hat{a}^\dagger)$ simultaneously couples both atomic transitions $|1\rangle - |2\rangle$ (frequency ω_{21}) and $|2\rangle - |3\rangle$ (frequency ω_{31}) with the corresponding detunings $\Delta_c = \omega_l - \omega_{21}$ and $\Delta_p = \omega_l - \omega_{32}$, respectively. The atom-cavity coupling strengths corresponding to respective atomic transitions are given by g_1 and g_2 .

compared with the Λ -type system. As we see below, since the two-photon Raman transition of a ladder-type atom can consume a pair of intracavity photons simultaneously, the collective atom-cavity coupling strength is enhanced by a factor of \sqrt{N} compared with that in the Λ -type system, which results in a significant reduction of the critical system size N_c for the superradiant phase transition. Like the previous section, both nondissipative and dissipative cases are discussed in detail and the spectroscopic properties of the output field are studied as well.

A. Physical model

The schematic diagram of the physical setup is the same as that in Fig. 1(a) except the intracavity particles are replaced by the three-level ladder-type atoms. As shown in Fig. 9, the ladder-type atomic system is composed of $|1, 2, 3\rangle$ states, where two single-photon transitions $|1\rangle - |2\rangle$ (frequency ω_{21}) and $|2\rangle - |3\rangle$ (frequency ω_{32}) are coupled simultaneously to the single-mode cavity [photon operators (a, a^\dagger) and frequency ω_l] with respective detunings $\Delta_c = \omega_l - \omega_{21}$ and $\Delta_p = \omega_l - \omega_{32}$. The corresponding atom-cavity interaction strengths are, respectively, given by g_1 and g_2 .

In the RWA, the Hamiltonian describing the coherent atom-cavity interaction can be expressed as

$$\begin{aligned} \hat{H}/\hbar = & \Delta_c \hat{J}_{1,1} - \Delta_p \hat{J}_{3,3} + \beta(\hat{a}^\dagger \hat{a}^\dagger + \hat{a} \hat{a}) \\ & + g_1(\hat{a}^\dagger \hat{J}_{1,2} + \hat{J}_{1,2}^\dagger \hat{a}) + g_2(\hat{a}^\dagger \hat{J}_{2,3} + \hat{J}_{2,3}^\dagger \hat{a}) \end{aligned}$$

in the interaction representation. The collective atomic operators $\hat{J}_{\mu,\nu}$ have been defined in the previous section. The third term on the right side of the equal sign denotes the nonlinear optical parametric oscillation in the parametric approximation [21].

Here we assume that the optical cavity far-off-resonantly interacts with both atomic transitions, i.e., $\Delta_c \gg g_1$ and $\Delta_p \gg g_2$, for which one can adiabatically eliminate the dynamics associated with the $|2\rangle$ state via the Schrieffer-Wolff transformation and obtain the effective Hamiltonian

(the spin-boson model)

$$\begin{aligned} \hat{H}/\hbar \approx & -\delta_R \hat{J}_z + g_R \left(\frac{\hat{J}_+}{N} a a + a^\dagger a^\dagger \frac{\hat{J}_-}{N} \right) \\ & + \left(\omega_{2,x} - \omega_{1,x} \frac{\hat{J}_z}{N} \right) \frac{(\hat{a}^\dagger + \hat{a})^2}{4} \\ & + \left(\omega_{2,y} - \omega_{1,y} \frac{\hat{J}_z}{N} \right) \frac{[i(\hat{a}^\dagger - \hat{a})]^2}{4}, \end{aligned} \quad (56)$$

where the ladder-type Raman-transition detuning δ_R is defined as

$$\delta_R = \Delta_c + \Delta_p - \frac{1}{2} \left(\frac{g_1^2}{\Delta_c} - \frac{g_2^2}{\Delta_p} \right), \quad (57)$$

the collective Raman-transition strength is given by

$$g_R = \frac{N g_1 g_2}{2 \Delta_c \Delta_p} (\Delta_p - \Delta_c), \quad (58)$$

the light shifts by $\omega_{1,x} = \frac{N g_1^2}{\Delta_c} (1 - \frac{2\beta}{\Delta_c}) + \frac{N g_2^2}{\Delta_p} (1 - \frac{2\beta}{\Delta_p})$ and $\omega_{1,y} = \frac{N g_1^2}{\Delta_c} (1 + \frac{2\beta}{\Delta_c}) + \frac{N g_2^2}{\Delta_p} (1 + \frac{2\beta}{\Delta_p})$, and the frequencies by $\omega_{2,x} = 2\beta + \frac{g_1^2}{2\Delta_c} (1 - \frac{2\beta}{\Delta_c}) - \frac{g_2^2}{2\Delta_p} (1 - \frac{2\beta}{\Delta_p})$ and $\omega_{2,y} = -2\beta + \frac{g_1^2}{2\Delta_c} (1 + \frac{2\beta}{\Delta_c}) - \frac{g_2^2}{2\Delta_p} (1 + \frac{2\beta}{\Delta_p})$. The collective atomic operator $\hat{J}_z = \frac{1}{2}(\hat{J}_{3,3} - \hat{J}_{1,1})$ measures the inversion of atoms between |1⟩ (spin-down) and |3⟩ (spin-up) states while $\hat{J}_+ = \hat{J}_{3,1}$ and $\hat{J}_- = \hat{J}_{1,3}$ are the raising and lowering angular momentum operators, respectively.

As one can see, unlike the spin-boson model of the Λ -type system [see Eq. (7)], no counter-rotating atom-cavity interaction terms exist in Eq. (56). Thus, in the ladder-type system only the parametric down-conversion process leads to the generation of intracavity photons, and the atomic Raman transition from the spin-down |1⟩ state to the spin-up |3⟩ state always consumes intracavity photons. As we see below, this leads to a different behavior of the influence of the cavity dissipation on the threshold of the superradiant phase transition compared with that of the Λ -type system.

In addition, the second term on the right side of the equal sign in Eq. (56) indicates the collective two-photon processes, i.e., one atom in the spin-down |1⟩ (or spin-up |3⟩) state absorbs (or emits) two intracavity photons and then transits to the spin-up |3⟩ (or spin-down |1⟩) state. Due to this two-photon Raman transition, the corresponding collective atom-cavity interaction strength g_R is proportional to the system size denoted by N . Compared with g_R in the Λ -type system [see Eq. (4)], the collective atom-cavity interaction strength g_R [see Eq. (58)] in the ladder-type system is amplified by a factor of \sqrt{N} , which results in a significant reduction of the threshold of the superradiant phase transition.

In the following, based on the spin-boson Hamiltonian (56) we investigate the superradiant phase transitions in both nondissipative and dissipative systems.

B. Superradiant phase transition in a nondissipative system

We first consider an ideal case, where no dissipation due to the spontaneous emission of atoms and cavity loss is involved in the atom-cavity dynamics. Similar to the previous

section, we are interested in the properties of the coupled system in the limit of a large number of atoms. In this case, we utilize again the Holstein-Primakoff transformation [26] and the displacement operators $D(\sqrt{N}A)$ and $D(\sqrt{N}B)$ to map the spin-boson Hamiltonian (56) into the two-mode boson representation [see Eq. (8)]. Further, we expand the displaced Hamiltonian $\hat{\mathcal{H}}$ up to second order in the boson operators [for example, see Eq. (9)] and obtain approximately $\hat{\mathcal{H}} \approx \mathcal{E}_0 + \hat{\mathcal{H}}_1 + \hat{\mathcal{H}}_2$.

The constant \mathcal{E}_0 , which gives the ground-state energy of the collectively coupled system, is expressed as

$$\begin{aligned} \frac{\mathcal{E}_0}{N\hbar} = & -(\delta_R + \omega_{1,x} X_A^2 + \omega_{1,y} Y_A^2) n_b \\ & + \left(\omega_{2,x} + \frac{\omega_{1,x}}{2} \right) X_A^2 + \left(\omega_{2,y} + \frac{\omega_{1,y}}{2} \right) Y_A^2 \\ & + 2g_R X_B \sqrt{1-n_b} (X_A^2 - Y_A^2) + 4g_R X_A Y_A Y_B \sqrt{1-n_b}, \end{aligned} \quad (59)$$

where the variables $X_{A,B}$ and $Y_{A,B}$ have been defined in the previous section. $n_a = X_A^2 + Y_A^2$ and $n_b = X_B^2 + Y_B^2$ give the mean values of the macroscopic occupations of the intracavity photons and atoms in the spin-up |3⟩ state. By choosing $X_{A,B}$ and $Y_{A,B}$ satisfying the following set of equations,

$$\begin{aligned} \left(\omega_{2,x} + \frac{\omega_{1,x}}{2} - \omega_{1,x} n_b \right) X_A \\ + 2g_R \sqrt{1-n_b} (X_A X_B + Y_A Y_B) = 0, \end{aligned} \quad (60)$$

$$\begin{aligned} \left(\omega_{2,y} + \frac{\omega_{1,y}}{2} - \omega_{1,y} n_b \right) Y_A \\ + 2g_R \sqrt{1-n_b} (X_A Y_B - Y_A X_B) = 0, \end{aligned} \quad (61)$$

$$\begin{aligned} (\delta_R + \omega_{1,x} X_A^2 + \omega_{1,y} Y_A^2) X_B + 2g_R \frac{X_A Y_A X_B Y_B}{\sqrt{1-n_b}} \\ - g_R (X_A^2 - Y_A^2) \left(\sqrt{1-n_b} - \frac{X_B^2}{\sqrt{1-n_b}} \right) = 0, \end{aligned} \quad (62)$$

$$\begin{aligned} (\delta_R + \omega_{1,x} X_A^2 + \omega_{1,y} Y_A^2) Y_B + g_R (X_A^2 - Y_A^2) \frac{X_B Y_B}{\sqrt{1-n_b}} \\ - 2g_R X_A Y_A \left(\sqrt{1-n_b} - \frac{Y_B^2}{\sqrt{1-n_b}} \right) = 0, \end{aligned} \quad (63)$$

the linear term $\hat{\mathcal{H}}_1$ in the displaced Hamiltonian $\hat{\mathcal{H}}$ vanishes. The quadratic term $\hat{\mathcal{H}}_2$ is considered below.

I. Ground state

We restrict ourselves to the case of $\Delta_c < 0$, $\Delta_p > 0$, and $g_1 = g_2 = g$, and one can apply the same approach to analyze other cases. It is easy to verify that the trivial solutions $X_{A,B} = Y_{A,B} = 0$ always satisfy Eqs. (60)–(63) and the corresponding ground-state energy is $\mathcal{E}_0 = 0$, which denotes the normal phase of the system; i.e., all atoms stay in the spin-down |1⟩ state and no photons exist inside cavity. Additionally, we obtain the other set of nontrivial solutions, i.e., $X_{A,B} \neq 0$, $Y_{A,B} = 0$, and

the average occupations

$$n_b = \frac{-P_b - \sqrt{P_b^2 - 4P_a P_c}}{2P_a}, \quad (64)$$

$$n_a = -\frac{\delta_R \sqrt{n_b(1-n_b)}}{\omega_{1,x} \sqrt{n_b(1-n_b)} + g_R(1-2n_b)}, \quad (65)$$

where $P_a = 1 + (\frac{\omega_{1,x}}{2g_R})^2$, $P_b = -1 - \frac{\omega_{1,x}}{2g_R}(\frac{\omega_{2,x}}{g_R} + \frac{\omega_{1,x}}{2g_R})$, and $P_c = \frac{1}{4}(\frac{\omega_{2,x}}{g_R} + \frac{\omega_{1,x}}{2g_R})^2$. Further, the corresponding ground-state energy is given by

$$\frac{\mathcal{E}_0}{N\hbar} = -\delta_R n_b + \left(\frac{\omega_{1,x}}{2} + \omega_{2,x} - \omega_{1,x} n_b \right) n_a - 2g_R n_a \sqrt{n_b(1-n_b)}. \quad (66)$$

For $n_{a,b} > 0$, one obtains $\mathcal{E}_0 < 0$, which means the system transits in a new phase; i.e., the macroscopic occupations in both intracavity field and pseudoangular momentum. Due to the adiabatic limit $|\Delta_{p,c}| \gg g_{1,2}$, the collective atom-cavity interaction g_R cannot be adjusted in a wide range by changing the coupling strengths $g_{1,2}$. Thus, in the following we amplify the collective atom-cavity interaction strength g_R via enlarging the system size N .

Figure 10(a) displays an example of $n_{a,b}$ changing with the number of atoms inside the cavity. As one can see, there exists a critical point N_c , after which the ground-state energy \mathcal{E}_0 becomes negative [see Fig. 10(b)]; i.e., the system undergoes a superradiant phase transition. From the analysis of the first- and second-order derivatives of \mathcal{E}_0 around the critical point [see Figs. 10(c) and 10(d)], the second-order phase transition is confirmed. For $N < N_c$, there are no intracavity photons

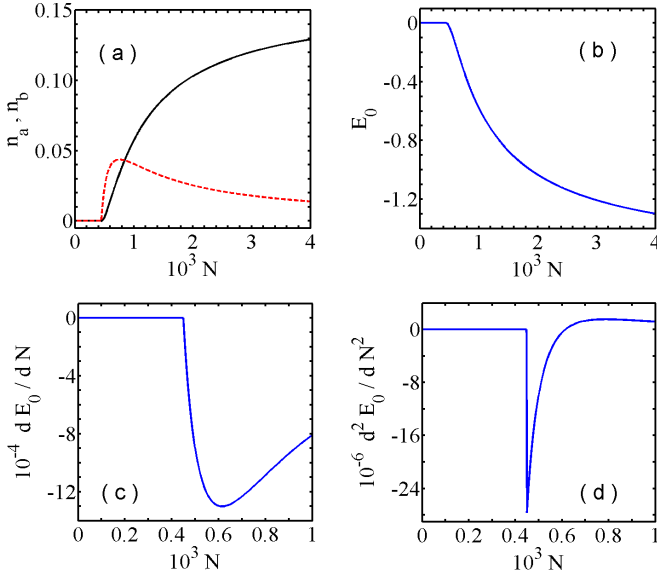


FIG. 10. (Color online) (a) n_b (solid line) and n_a (dashed line) as a function of the system size N . The corresponding average ground-state energy $E_0 = \frac{\mathcal{E}_0}{N\hbar g}$ is shown in panel (b). When N is larger than the critical atomic number $N_c \approx 4.5 \times 10^2$, E_0 becomes negative. The first and second derivatives of the ground-state energy with respect to N around N_c are displayed in panels (c) and (d), respectively. For all curves, $\Delta_c = -20g$, $\Delta_p = 30g$, $\beta = 10g$, and $g_1 = g_2 = g$.

or excited atoms. When $N > N_c$, more and more atoms are populated in the spin-up $|3\rangle$ state while the intracavity field is first amplified and then goes down as the system size N is further enlarged.

For a small number of atoms, the relative larger Raman-transition detuning δ_R impedes the two-photon excitation of atoms from $|1\rangle$ to $|3\rangle$ and in turn this suppression of atomic excitation blocks the degenerate parametric down-conversion process. In this case, the system is in the normal phase $\mathcal{E}_0 = n_a = n_b = 0$. Since the collective atom-cavity interaction g_R is proportional to N , the strongly coupled regime of the composite system can be reached as N is increased. When $N > N_c$, the strong atom-cavity interaction overcomes the large Raman-transition detuning δ_R and a collective intracavity dynamics is rapidly established, which results in $n_{a,b} > 0$. As g_R is further increased for a larger N , it no longer requires a large number of intracavity photons to support the collective atom-cavity dynamics. Thus, the intracavity field goes down while n_b keeps climbing up [see Fig. 10(a)].

Comparing Fig. 10(a) with Fig. 2(a), we find that the behaviors of $n_{a,b}$ versus the system size N in two different collectively coupled systems are alike. This is because the fundamental models of these two composite systems are similar, i.e., the collective Raman transition plus the nonlinear parametric oscillation. Nevertheless, the critical system size N_c for the ladder-type system is obviously much smaller than that for the Λ -type system. As we have pointed out, this is primarily because the collective atom-cavity interaction strength g_R [Eq. (58)] in the ladder-type system is strongly enhanced by a factor of \sqrt{N} due to the two-photon Raman transition compared with that for the Λ -type system [Eq. (4)]. For this reason, even a much smaller intracavity light field can maintain a strong collective atom-cavity dynamics in the ladder-type system, which makes the superradiant phase transition occur more easily.

Figures 11(a) and 11(b) show the dependence of $n_{a,b}$ on the Raman-transition detuning δ_R for different N . For a fixed N , at which the system is in the superradiant phase, enlarging δ_R enhances both the intracavity field and atomic population inversion. This is because more photons inside the cavity are needed so as to maintain the strong collective atom-cavity dynamics and in return more atoms are excited to the spin-up state. Moreover, from the expression of the ground-state energy (66) one finds that the larger δ_R profits from the occurrence of the superradiant phase transition. However, δ_R cannot be increased very much since the effective Hamiltonian (56) is only valid to the second-order terms of g_1^2/Δ_c and g_2^2/Δ_p . Moreover, from Eq. (64) we can numerically investigate the critical system size N_c for the superradiant phase transition and the results are shown in Fig. 11(c). As one can see, increasing either β or δ_R raises N_c because of the enlarged light shifts and Raman detuning.

2. Elementary excitations

So far, we have only discussed the ground state of the coupled system. Now we consider the elementary excitations of the composite system in different phases, which are closely tied up with the system parity. The quadratic term $\hat{\mathcal{H}}_2$ in the expansion of the Hamiltonian $\hat{\mathcal{H}}$ can be written in a general

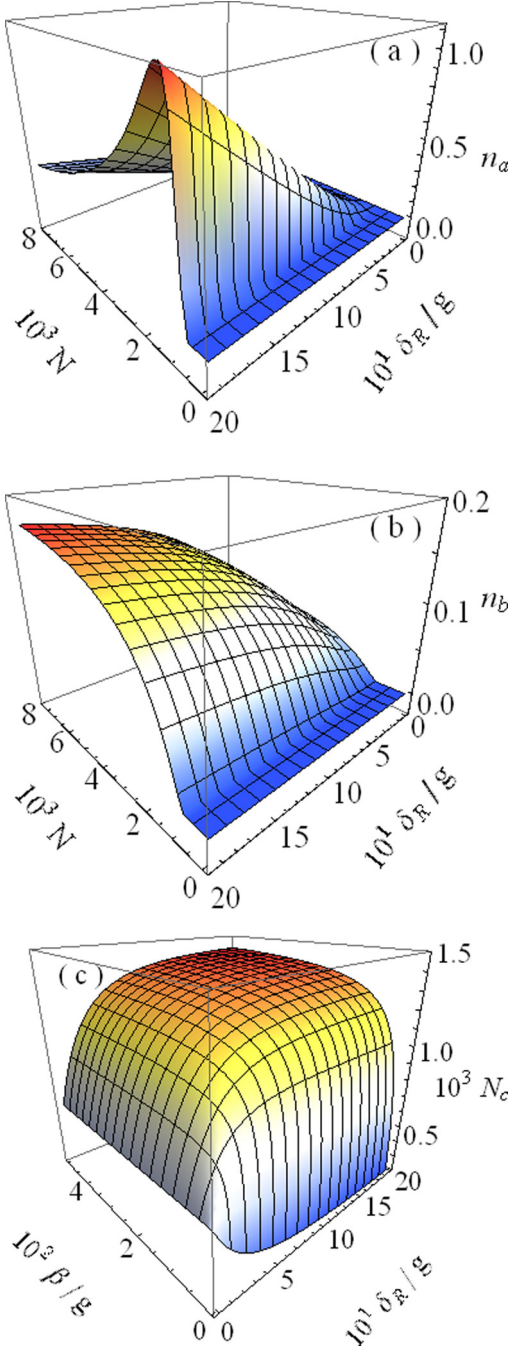


FIG. 11. (Color online) Macroscopic occupations n_a (a) and n_b (b) as a function of the system size N and the Raman-transition detuning δ_R , where $\Delta_c = -30g$ and $\beta = 10g$. (c) The dependence of the critical system size N_c on β and δ_R . For all figures, δ_R is adjusted by changing Δ_p .

form same to Eq. (21), where we have defined the parameters $u_+ = \frac{1}{4}[-\omega_{1,x}n_b + \frac{\omega_{1,x}}{2} + \omega_{2,x} - 2g_R\sqrt{n_b(1-n_b)}]$, $u_- = \frac{1}{4}[-\omega_{1,y}n_b + \frac{\omega_{1,y}}{2} + \omega_{2,y} + 2g_R\sqrt{n_b(1-n_b)}]$, $v_+ = \frac{1}{4}[-\delta_R - \omega_{1,x}n_a - g_Rn_a\sqrt{n_b\frac{(-3+2n_b)}{(1-n_b)^{3/2}}}]$, $v_- = \frac{1}{4}[-\delta_R - \omega_{1,x}n_a + g_Rn_a\sqrt{\frac{n_b}{1-n_b}}]$, $\lambda_+ = \omega_{1,x}\sqrt{n_a n_b} + g_R\sqrt{n_a\frac{1-2n_b}{\sqrt{1-n_b}}}$, and $\lambda_- = g_R\sqrt{n_a(1-n_b)}$.

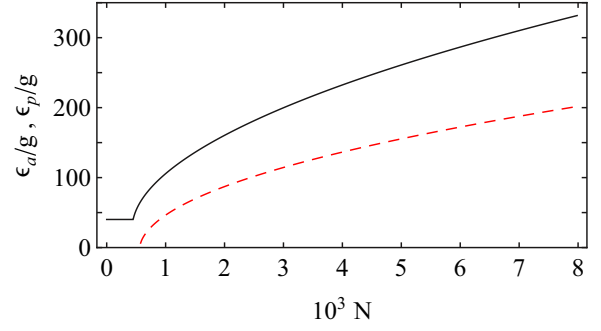


FIG. 12. (Color online) The elementary excitation spectrum corresponding to Fig. 10 as a function of the system size N . The solid and dash lines denote ϵ_a and ϵ_p , respectively.

$\hat{\mathcal{H}}_2$ can be diagonalized as Eq. (28) via the Bogoliubov transformation [see Eqs. (22)–(26)]. $\epsilon_{a,p}$ give the atomic and photonic branches of elementary excitations according to their values for $N \rightarrow 0$ [15]. $\hat{e}_{a,p}$ and $\hat{e}_{a,p}^\dagger$ are the corresponding annihilation and creation operators.

Figure 12 displays a sample of two excitation branches $\epsilon_{a,p}$ as a function of the system size N . For a system in the normal phase, only the atomic branch of elementary excitation ϵ_a , which is always equal to δ_R , exists while the photonic excitation branch ϵ_p is invalid. Unlike the Λ -type system (see Fig. 4), here both branches of excitation energies are valid in the superradiant phase and $\epsilon_{a,p}$ go up as more atoms are involved inside the cavity. Thus, the elementary excitation spectrum strongly depends on the specific atomic structure.

Finally, we are aware that the occurrence of the superradiant phase transition is accompanied by the symmetry breaking of the global parity operator $\hat{\Pi}$. For the system in the normal phase $\hat{\Pi}$ is expressed as $\hat{\Pi} = \exp(i\pi\hat{\Xi})$, where $\hat{\Xi} = \hat{a}^\dagger\hat{a} + \hat{J}_z + N$ counts the total number of excitation quanta in the system [27] and $[\hat{H}, \hat{\Pi}] = 0$, while the local parity operator $\hat{\Pi}_2 = \exp[i\pi(\hat{e}_a^\dagger\hat{e}_a + \hat{e}_p^\dagger\hat{e}_p)]$ commutes with $\hat{\mathcal{H}}_2$ obviously for the system in the superradiant phase.

C. Dissipative atom-cavity system

Above, we focused on the collective coherent interaction between an ensemble of atoms and an ideal optical resonator. However, the atomic spontaneous emission and the cavity loss are unavoidable in reality and it is necessary to consider the influence of the dissipation on the collective atom-cavity dynamics. Here we should note that, unlike the Λ -type atomic system, the decay of the atomic polarization between the $|1\rangle$ and $|3\rangle$ states cannot be ignored due to the unavoidable spontaneous emission of atoms in the excited $|2\rangle$ and $|3\rangle$ states. Thus, the effect of the atomic spontaneous emission is considered here.

Generally, there are many decay channels in the atomic system. For the sake of simplicity, we introduce a decay rate γ to describe the effective loss of the coherence between the $|1\rangle$ and $|3\rangle$ states. This is valid when two detunings $\Delta_{c,p}$ are much larger than the polarization decay rates of two atomic $|1\rangle - |2\rangle$ and $|2\rangle - |3\rangle$ transitions, for which the dynamics related to the $|2\rangle$ state can still be adiabatically eliminated and the spin-boson Hamiltonian (56) is valid in the dissipative case.

In addition, we assume that only one of the cavity mirrors is partially reflective and the resulting cavity damping rate is κ .

Following the same method in Refs. [30–33], one can find the quantum Langevin equations of the intracavity field and atomic operators:

$$\begin{aligned} \frac{d}{dt} \hat{j}_x(t) = & -\frac{\gamma}{2} \hat{j}_x(t) + [\delta_R + \omega_{1,x} \hat{x}_a^2(t) + \omega_{1,y} \hat{y}_a^2(t)] \hat{j}_y(t) \\ & - 2g_R \{\hat{x}_a(t), \hat{y}_a(t)\} \hat{j}_z(t) + \hat{f}_x(t), \end{aligned} \quad (67)$$

$$\begin{aligned} \frac{d}{dt} \hat{j}_y(t) = & -\frac{\gamma}{2} \hat{j}_y(t) - [\delta_R + \omega_{1,x} \hat{x}_a^2(t) + \omega_{1,y} \hat{y}_a^2(t)] \hat{j}_x(t) \\ & - 2g_R [x_a^2(t) - y_a^2(t)] \hat{j}_z(t) + \hat{f}_y(t), \end{aligned} \quad (68)$$

$$\begin{aligned} \frac{d}{dt} \hat{j}_z(t) = & -\frac{\gamma}{2} - \gamma \hat{j}_z(t) + 2g_R [x_a^2(t) - y_a^2(t)] \hat{j}_y(t) \\ & + 2g_R \{\hat{x}_a(t), \hat{y}_a(t)\} \hat{j}_x(t) + \hat{f}_z(t), \end{aligned} \quad (69)$$

$$\begin{aligned} \frac{d}{dt} \hat{x}_a(t) = & -\frac{\kappa}{2} \hat{x}_a(t) - [\omega_{1,y} \hat{j}_z(t) + 2g_R \hat{j}_x(t)] \hat{y}_a(t) \\ & + \omega_{2,y} \hat{y}_a(t) - 2g_R \hat{x}_a(t) \hat{j}_y(t) + \hat{f}_{\kappa,x}(t), \end{aligned} \quad (70)$$

$$\begin{aligned} \frac{d}{dt} \hat{y}_a(t) = & -\frac{\kappa}{2} \hat{y}_a(t) + [\omega_{1,x} \hat{j}_z(t) - 2g_R \hat{j}_x(t)] \hat{x}_a(t) \\ & - \omega_{2,x} \hat{x}_a(t) + 2g_R \hat{y}_a(t) \hat{j}_y(t) + \hat{f}_{\kappa,y}(t), \end{aligned} \quad (71)$$

where the anticommutator

$$\{\hat{x}_a(t), \hat{y}_a(t)\} = \hat{x}_a(t) \hat{y}_a(t) + \hat{y}_a(t) \hat{x}_a(t). \quad (72)$$

The definitions of operators $\hat{j}_{x,y,z}(t)$, $\hat{x}_a(t)$, and $\hat{y}_a(t)$ are same as those in the previous section. The above Heisenberg-Langevin equations have the same structure,

$$\frac{d}{dt} \hat{O}(t) = A_O(t) + \hat{f}_O(t), \quad (73)$$

where $A_O(t)$ is the deterministic part of the equation and $\hat{f}_O(t)$ is the quantum noise operator, which satisfies $\langle \hat{f}_O(t) \rangle = 0$. Here, we list the nonvanishing intercorrelations $\langle \hat{j}_x(t) \hat{j}_x(t') \rangle = \frac{\gamma}{4N} \delta(t-t')$, $\langle \hat{j}_x(t) \hat{f}_y(t') \rangle = -\frac{i\gamma}{4N} \delta(t-t')$, $\langle \hat{j}_x(t) \hat{f}_z(t') \rangle = \frac{\gamma}{2N} [\langle \hat{j}_x(t) \rangle - i \langle \hat{j}_y(t) \rangle] \delta(t-t')$, $\langle \hat{j}_y(t) \hat{f}_x(t') \rangle = \frac{i\gamma}{4N} \delta(t-t')$, $\langle \hat{j}_y(t) \hat{f}_y(t') \rangle = \frac{\gamma}{4N} \delta(t-t')$, $\langle \hat{j}_{\kappa,x}(t) \hat{f}_{\kappa,x}(t') \rangle = \frac{\kappa}{4N} \delta(t-t')$, $\langle \hat{j}_y(t) \hat{f}_z(t') \rangle = \frac{i\gamma}{2N} [\langle \hat{j}_x(t) \rangle - i \langle \hat{j}_y(t) \rangle] \delta(t-t')$, $\langle \hat{f}_{\kappa,y}(t) \hat{f}_{\kappa,y}(t') \rangle = \frac{\kappa}{4N} \delta(t-t')$, $\langle \hat{f}_z(t) \hat{f}_x(t') \rangle = \frac{\gamma}{2N} [\langle \hat{j}_x(t) \rangle + i \langle \hat{j}_y(t) \rangle] \delta(t-t')$, $\langle \hat{f}_{\kappa,x}(t) \hat{f}_{\kappa,y}(t') \rangle = \frac{i\kappa}{4N} \delta(t-t')$, $\langle \hat{f}_z(t) \hat{f}_y(t') \rangle = -\frac{i\gamma}{2N} [\langle \hat{j}_x(t) \rangle + i \langle \hat{j}_y(t) \rangle] \delta(t-t')$, $\langle \hat{f}_{\kappa,y}(t) \hat{f}_{\kappa,x}(t') \rangle = -\frac{i\kappa}{4N} \delta(t-t')$, and $\langle \hat{f}_z(t) \hat{f}_z(t') \rangle = \frac{\gamma}{N} (\langle \hat{j}_z(t) \rangle + \frac{1}{2}) \delta(t-t')$. The above intercorrelation functions can be written in a general form,

$$\langle \hat{f}_\mu(t) \hat{f}_\nu(t') \rangle = 2D_{\mu,\nu} \delta(t-t'), \quad (74)$$

where $2D_{\mu,\nu}$ is the diffusion coefficient in the fluctuation-dissipation theorem.

1. Steady-state solutions

First, we consider the steady state of the atom-cavity system. By introducing the c -number variables $O(t) = \langle \hat{O}(t) \rangle$ and

neglecting quantum fluctuations $\langle \hat{O}_1(t) \hat{O}_2(t) \rangle \approx O_1(t) O_2(t)$, the quantum Langevin equations (67)–(71) can be converted into a set of differential equations:

$$\begin{aligned} \frac{d}{dt} j_x(t) = & -\frac{\gamma}{2} j_x(t) + [\delta_R + \omega_{1,x} x_a^2(t) + \omega_{1,y} y_a^2(t)] j_y(t) \\ & - 4g_R x_a(t) y_a(t) j_z(t), \end{aligned} \quad (75)$$

$$\begin{aligned} \frac{d}{dt} j_y(t) = & -\frac{\gamma}{2} j_y(t) - [\delta_R + \omega_{1,x} x_a^2(t) + \omega_{1,y} y_a^2(t)] j_x(t) \\ & - 2g_R [x_a^2(t) - y_a^2(t)] j_z(t), \end{aligned} \quad (76)$$

$$\begin{aligned} \frac{d}{dt} j_z(t) = & -\frac{\gamma}{2} - \gamma j_z(t) + 2g_R [x_a^2(t) - y_a^2(t)] j_y(t) \\ & + 4g_R x_a(t) y_a(t) j_x(t), \end{aligned} \quad (77)$$

$$\begin{aligned} \frac{d}{dt} x_a(t) = & -\frac{\kappa}{2} x_a(t) + [\omega_{2,y} - \omega_{1,y} j_z(t) - 2g_R j_x(t)] y_a(t) \\ & - 2g_R x_a(t) j_y(t), \end{aligned} \quad (78)$$

$$\begin{aligned} \frac{d}{dt} y_a(t) = & -\frac{\kappa}{2} y_a(t) - [\omega_{2,x} - \omega_{1,x} j_z(t) + 2g_R j_x(t)] x_a(t) \\ & + 2g_R y_a(t) j_y(t). \end{aligned} \quad (79)$$

Moreover, the above semiclassical equations conserve the pseudoangular momentum $j_x^2(t) + j_y^2(t) + j_z^2(t) = \frac{1}{4}$.

The steady-state solutions for the mean values of the intracavity field and atomic variables can be solved by setting $\frac{d}{dt} O(t) = 0$ in Eqs. (75)–(79). These solutions are denoted by the subscript “ o ”. Directly deriving the analytical solutions from the semiclassical equations is particularly difficult. Here we exploit the numerical method to solve the steady states of the composite system.

Figure 13 shows the dependence of the mean values of the steady-state intracavity photons $n_a = x_{a,o}^2 + y_{a,o}^2$ and atomic inversion $n_b = j_{z,o} + 0.5$ on γ and κ . As one can see, for a fixed γ enlarging the cavity loss rate κ reduces both intracavity field and atomic population in the spin-up $|3\rangle$ state since the portion of photons produced via the degenerate parametric down-conversion process escape the optical cavity without interacting with atoms. In contrast, for a fixed κ , n_a is amplified while n_b goes down as γ is increased. This is because atoms in $|1\rangle$ are hardly excited to $|3\rangle$ and atoms in $|3\rangle$ rapidly decay back to $|1\rangle$ for a larger γ , which indicates the atoms rarely interact with the optical resonator. As a consequence, more photons accumulate inside the cavity and the intracavity field is enhanced.

One can derive the threshold N_c of the superradiant phase transition by numerically solving Eqs. (75)–(79). Figure 14 illustrates the dependence of N_c on the cavity loss rate κ for several different atomic spontaneous emission rates γ . We find that, unlike the Λ -type system (see Fig. 6), N_c goes up as κ is increased for a fixed γ . This can be understood from the difference between the collective atom-cavity interactions of those two systems [see Eqs. (7) and (56)].

We assume that for the system being in a steady state there is a small increase of the cavity loss rate κ . In this case, more photons should be generated via the nonlinear parametric

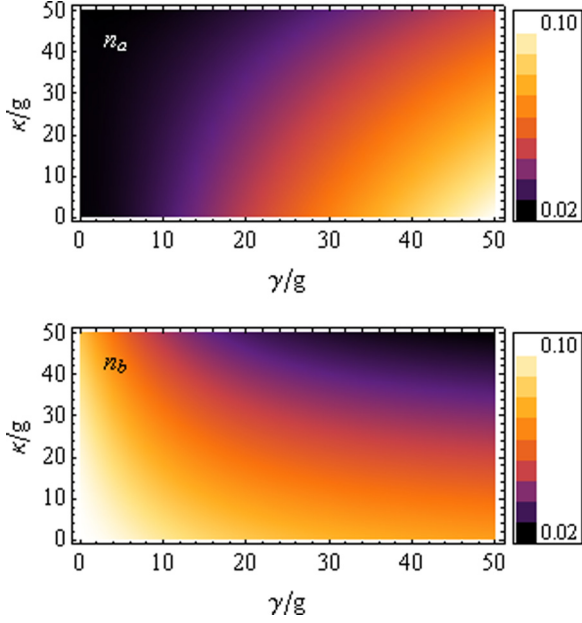


FIG. 13. (Color online) The steady-state n_a and n_b as a function of the effective decay rate γ and the cavity loss rate κ . The system size is set at $N = 2 \times 10^3$ and all the other parameters are the same as those in Fig. 11.

oscillation so as to compensate for the increased loss of intracavity field. This compensation process is strongly enhanced due to the counter-rotating interaction terms in Hamiltonian (3); i.e., the Raman transition of atoms from the spin-down $|2\rangle$ state to the spin-up $|1\rangle$ state amplifies the intracavity field. Thus, in the new steady state of the system, more atoms populate in the spin-up state and more photons accumulate inside the optical resonator for the Λ -type system. Further, the threshold of the superradiant phase transition is reduced. However, the situation is completely different for the ladder-type system, where no counter-rotating atom-cavity interaction terms exist in the Hamiltonian (56). Since the ladder-type atomic Raman transition from the spin-down $|1\rangle$ state to the spin-up $|3\rangle$ state always consumes the intracavity photons, the generation of the

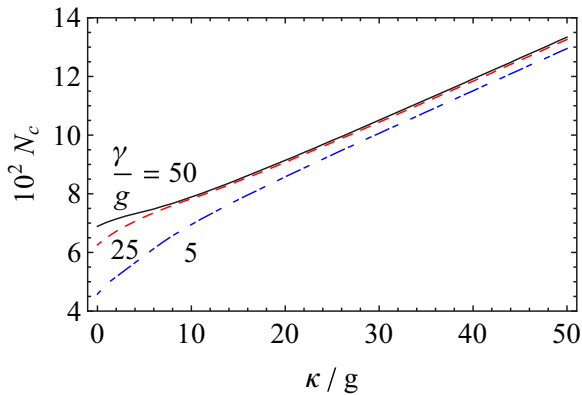


FIG. 14. (Color online) The threshold of the superradiant phase transition as a function of the cavity loss rate κ for several different decay rates γ . All the other parameters are the same as those in Fig. 11.

intracavity photons via the nonlinear parametric oscillation is strongly suppressed. As a result, the threshold N_c grows as κ is increased.

Finally, we find that increasing the atomic spontaneous emission rate γ raises the threshold of the phase transition. Since atoms are hardly excited for a larger γ , more atoms stay in the spin-down $|1\rangle$ state, which results in a higher threshold. In addition, as shown in Fig. 14, the atomic spontaneous emission mainly affects the threshold N_c for a small κ .

2. Stability analysis

It is essential to consider the stability of the derived steady-state solutions, for which we assume that the operator variable $\hat{O}(t)$ can be presented as a sum of the dominant classical term O_o and a small fluctuation $\delta\hat{O}(t)$, $\hat{O}(t) \approx O_o + \delta\hat{O}(t)$. In this case, the quantum Langevin equations (67)–(71) can be linearized and we obtain the following equations for the fluctuations:

$$\begin{aligned} \frac{d}{dt}\delta\hat{j}_x(t) = & -\frac{\gamma}{2}\delta\hat{j}_x(t) + (\delta_R + \omega_{1,x}x_{a,o}^2 + \omega_{1,y}y_{a,o}^2)\delta\hat{j}_y(t) \\ & + 2(\omega_{1,x}x_{a,o}j_{y,o} - 2g_R y_{a,o}j_{z,o})\delta\hat{x}_a(t) \\ & + 2(\omega_{1,y}y_{a,o}j_{x,o} - 2g_R x_{a,o}j_{z,o})\delta\hat{y}_a(t) \\ & - 4g_R x_{a,o}y_{a,o}\delta\hat{j}_z(t) + \hat{f}_x(t), \end{aligned} \quad (80)$$

$$\begin{aligned} \frac{d}{dt}\delta\hat{j}_y(t) = & -\frac{\gamma}{2}\delta\hat{j}_y(t) - (\delta_R + \omega_{1,x}x_{a,o}^2 + \omega_{1,y}y_{a,o}^2)\delta\hat{j}_x(t) \\ & - 2(\omega_{1,x}x_{a,o}j_{x,o} + 2g_R x_{a,o}j_{z,o})\delta\hat{x}_a(t) \\ & - 2(\omega_{1,y}y_{a,o}j_{x,o} - 2g_R y_{a,o}j_{z,o})\delta\hat{y}_a(t) \\ & - 2g_R(x_{a,o}^2 - y_{a,o}^2)\delta\hat{j}_z(t) + \hat{f}_y(t), \end{aligned} \quad (81)$$

$$\begin{aligned} \frac{d}{dt}\delta\hat{j}_z(t) = & -\gamma\delta\hat{j}_z(t) + 4g_R x_{a,o}y_{a,o}\delta\hat{j}_x(t) + 4g_R(x_{a,o}j_{y,o} \\ & + y_{a,o}j_{x,o})\delta\hat{x}_a(t) + 4g_R(x_{a,o}j_{x,o} - y_{a,o}j_{y,o}) \\ & \times \delta\hat{y}_a(t) + 2g_R(x_{a,o}^2 - y_{a,o}^2)\delta\hat{j}_y(t) + \hat{f}_z(t), \end{aligned} \quad (82)$$

$$\begin{aligned} \frac{d}{dt}\delta\hat{x}_a(t) = & -2g_R y_{a,o}\delta\hat{j}_x(t) - 2g_R x_{a,o}\delta\hat{j}_y(t) - \omega_{1,y}y_{a,o}\delta\hat{j}_z(t) \\ & - (-\omega_{2,y} + \omega_{1,y}j_{z,o} + 2g_R j_{x,o})\delta\hat{y}_a(t) \\ & - \left(\frac{\kappa}{2} + 2g_R j_{y,o}\right)\delta\hat{x}_a(t) + \hat{f}_{\kappa,x}(t), \end{aligned} \quad (83)$$

$$\begin{aligned} \frac{d}{dt}\delta\hat{y}_a(t) = & -2g_R x_{a,o}\delta\hat{j}_x(t) + 2g_R y_{a,o}\delta\hat{j}_y(t) + \omega_{1,x}x_{a,o}\delta\hat{j}_z(t) \\ & - (\omega_{2,x} - \omega_{1,x}j_{z,o} + 2g_R j_{x,o})\delta\hat{x}_a(t) \\ & - \left(\frac{\kappa}{2} - 2g_R j_{y,o}\right)\delta\hat{y}_a(t) + \hat{f}_{\kappa,y}(t). \end{aligned} \quad (84)$$

We write the above linear equations in the matrix form $\frac{d}{dt}\hat{\mathbf{v}}(t) = \mathbf{M}\hat{\mathbf{v}}(t) + \hat{\mathbf{f}}(t)$, where the column matrices

$$\begin{aligned} \hat{\mathbf{v}}(t) = & (\delta\hat{j}_x(t), \delta\hat{j}_y(t), \delta\hat{j}_z(t), \delta\hat{x}_a(t), \delta\hat{y}_a(t))^T, \\ \hat{\mathbf{f}}(t) = & (\hat{f}_x(t), \hat{f}_y(t), \hat{f}_z(t), \hat{f}_{\kappa,x}(t), \hat{f}_{\kappa,y}(t))^T, \end{aligned}$$

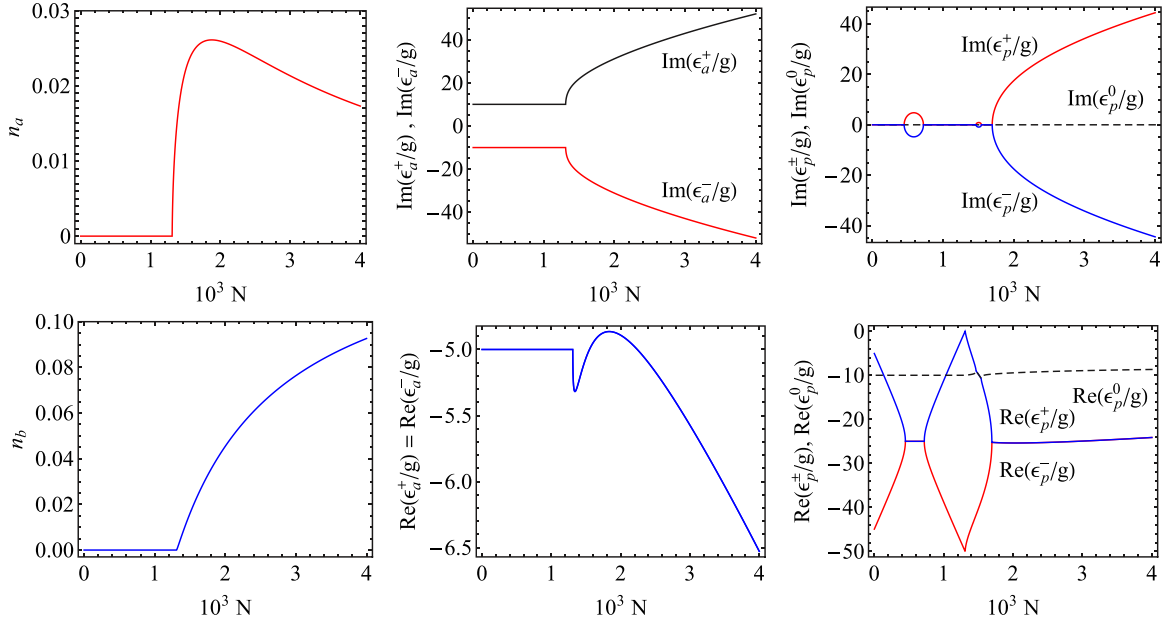


FIG. 15. (Color online) Steady-state solutions $n_{a,b}$, the corresponding decay rates $\text{Re}(\epsilon_a^\pm)$ and $\text{Re}(\epsilon_p^{\pm,0})$, and the corresponding elementary-excitation frequencies $\text{Im}(\epsilon_a^\pm)$ and $\text{Im}(\epsilon_p^0)$ as a function of the system size N . The critical point is localized at $N_c \approx 1.3 \times 10^3$. For all curves, $\gamma = 10g$ and $\kappa = 50g$ and all the other parameters are the same as those in Fig. 11.

and \mathbf{M} is a constant square matrix. Diagonalizing \mathbf{M} gives us five eigenvalues, which can be divided into two groups, i.e., ϵ_a^\pm associated with the atomic branch and the other three $\epsilon_p^{\pm,0}$ associated with the photonic branch according to the values in the limit of $N \rightarrow 0$. The stable steady-state solution requires that all the real parts of ϵ_a^\pm and $\epsilon_p^{\pm,0}$ be negative, i.e., $\text{Re}(\epsilon_a^\pm) < 0$ and $\text{Re}(\epsilon_p^{\pm,0}) < 0$. Additionally, the imaginary parts $\text{Im}(\epsilon_{a,p}^\pm)$ correspond to the excitation-energy shifts and $\text{Im}(\epsilon_p^0)$ is always zero. We can prove that as $\gamma \rightarrow 0$ and $\kappa \rightarrow 0$, $\epsilon_{a,p}^\pm$ are reduced to the elementary excitations $\epsilon_{a,p}$ in the nondissipative system and ϵ_p^0 approaches zero. Thus, the effects of the spontaneous emission of atoms and cavity loss split the elementary excitations and induce the finite lifetimes to the elementary excitations.

Figure 15 displays the dependence of different eigenvalues on the atomic number N . As one can see, two atomic branch excitations ϵ_a^\pm have the same decay rate, i.e., $\text{Re}(\epsilon_a^+) = \text{Re}(\epsilon_a^-)$, which is equal to $-\frac{\gamma}{2}$ for $N < N_c$ and approximately linearly increases when $N > N_c$, and opposite energy shifts, i.e., $\text{Im}(\epsilon_a^+) = -\text{Im}(\epsilon_a^-)$. For the photonic branch excitations, ϵ_p^\pm have the opposite excitation energies, i.e., $\text{Im}(\epsilon_p^+) = -\text{Im}(\epsilon_p^-)$, while the $\text{Im}(\epsilon_p^0)$ is always zero. Finally, the real parts of different photonic branch excitations are all negative, which means the steady-state solutions $n_{a,b}$ are stable.

3. Spectra of the output field

In the presence of cavity loss, vacuum fluctuations enter the cavity and influence the collective coherent atom-cavity interaction. In turn, the cavity loss offers access to monitor the composite system properties via the light field leaking out from the cavity mirror. According to the input-output theory, the Hermitian amplitude operators for the cavity output field

are given by

$$\hat{x}_{\text{out}}(t) = \sqrt{\kappa} \hat{x}_a(t) - \frac{\hat{f}_{\kappa,x}(t)}{\sqrt{\kappa}}, \quad \hat{y}_{\text{out}}(t) = \sqrt{\kappa} \hat{y}_a(t) - \frac{\hat{f}_{\kappa,y}(t)}{\sqrt{\kappa}}.$$

For a system in the stationary state, the output-field variables can be considered as a sum of the dominant value and a small fluctuation operator:

$$\delta \hat{x}_{\text{out}}(t) = \sqrt{\kappa} \delta \hat{x}_a(t) - \hat{f}_{\kappa,x}(t)/\sqrt{\kappa}, \quad (85)$$

$$\delta \hat{y}_{\text{out}}(t) = \sqrt{\kappa} \delta \hat{y}_a(t) - \hat{f}_{\kappa,y}(t)/\sqrt{\kappa}. \quad (86)$$

As one can see, the noise of the cavity output field originates from the intracavity fluctuations and the vacuum fluctuations outside the cavity.

The fluctuation of the intracavity field can be derived from the linear equations (80)–(84). It is convenient to convert this set of differential equations into equations in the frequency domain via the Fourier transform, Eqs. (52) and (53). For simplicity, we use the same symbol for both members of a Fourier-transform pair, which will be distinguished through the time or frequency argument. Further, it is easy to obtain the intercorrelations

$$\langle \hat{f}_\mu(\omega) \hat{f}_\nu(\omega') \rangle = 2D_{\mu,\nu} \delta(\omega + \omega'). \quad (87)$$

The homodyne spectra corresponding to the output-field quadrature amplitudes are defined as

$$S_0(\omega) = \int_{-\infty}^{+\infty} \langle \delta \hat{x}_{\text{out}}(t + \tau) \delta \hat{x}_{\text{out}}(t) \rangle e^{i\omega\tau} d\tau, \quad (88)$$

$$S_{\frac{\pi}{2}}(\omega) = \int_{-\infty}^{+\infty} \langle \delta \hat{y}_{\text{out}}(t + \tau) \delta \hat{y}_{\text{out}}(t) \rangle e^{i\omega\tau} d\tau, \quad (89)$$

where $S_0(\omega)$ denotes the spectrum of output-field amplitude fluctuations while $S_{\frac{\pi}{2}}(\omega)$ gives the phase-fluctuation spectrum.

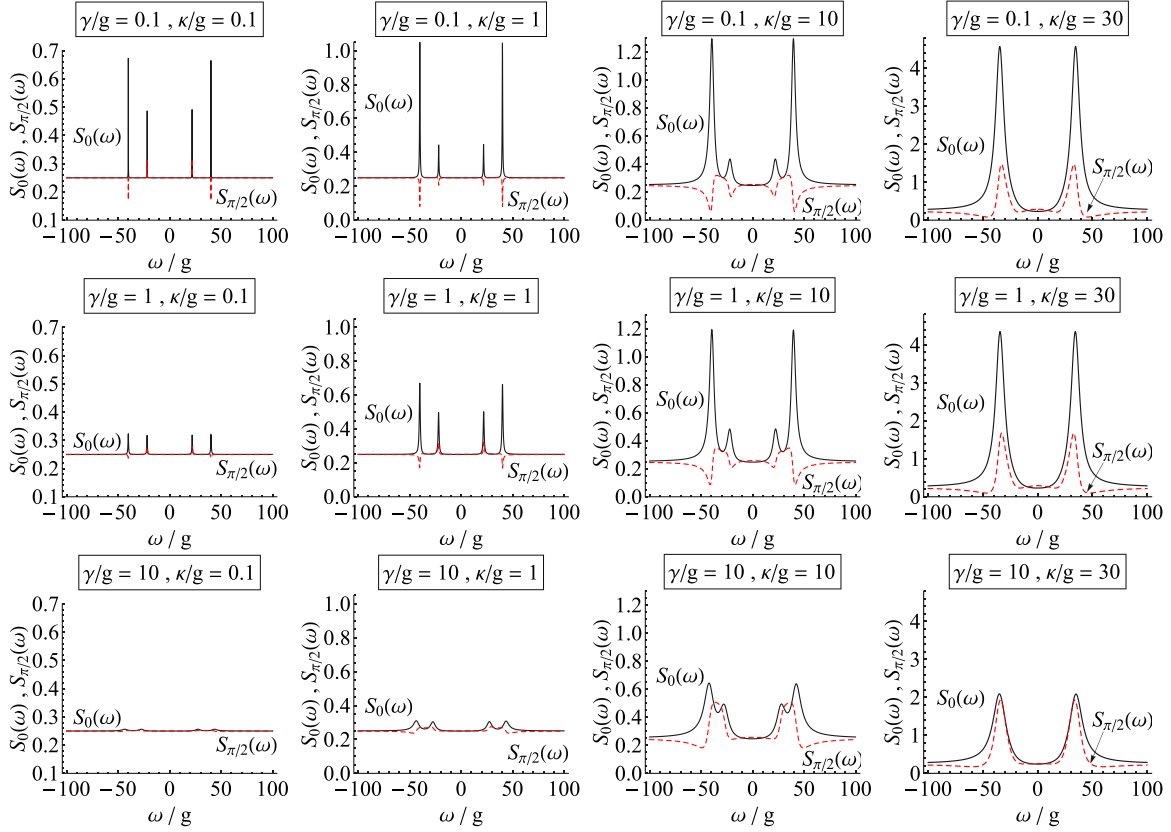


FIG. 16. (Color online) The output-field spectra of the amplitude and phase fluctuations $S_{0, \frac{\pi}{2}}(\omega)$ as a function of ω for different atomic decay rates γ and cavity losses κ . For all curves, $N = 2 \times 10^3$, at which the system is in the superradiant phase, and all the other parameters are the same as those in Fig. 2.

Figure 16 shows $S_0(\omega)$ and $S_{\frac{\pi}{2}}(\omega)$ for different γ and κ for a system in the superradiant phase ($N > N_c$). In either spectrum, there exist two pairs of spikes, where the outboard pair corresponds to the atomic branch elementary excitations ϵ_a^\pm while the inboard pair denotes the photonic branch excitations ϵ_p^\pm . Another photonic branch ϵ_p^0 is hardly presented in the spectra. From Fig. 16 we can obtain the following qualitative conclusions.

(i) For a fixed γ , when κ is reduced to zero one obtains four extremely narrow spikes in both spectra. In the amplitude spectrum $S_0(\omega)$, all spikes are higher than the shot-noise level arising from the vacuum fluctuations, i.e., $\frac{1}{4}$. However, the photonic branch pair in $S_{\frac{\pi}{2}}(\omega)$ are higher than $\frac{1}{4}$ while the atomic branch pair are lower than the shot-noise limit, which indicates a squeezing in the phase fluctuations around the photonic branch resonances.

(ii) For a larger cavity loss rate, the heights of two photonic branch spikes in $S_0(\omega)$ are suppressed while the atomic branch peaks are dramatically enhanced. Contrarily, all four spikes in the phase spectrum $S_{\frac{\pi}{2}}(\omega)$ are below the shot-noise level. As κ is increased, the noise reduction on the photonic branch resonances in $S_{\frac{\pi}{2}}(\omega)$ approaches 100%. Moreover, the widths of spikes in either spectrum are broadened.

(iii) As κ is further enlarged, the energy shifts $\text{Im}(\epsilon_a^\pm)$ and $\text{Im}(\epsilon_p^\pm)$ approach each other and the damping rates $\text{Re}(\epsilon_a^\pm)$ and $\text{Re}(\epsilon_p^\pm)$ are very large. Consequently, two spikes on either side, for example, ϵ_a^+ and ϵ_p^+ , overlap each other and form a huge spike. The four-peaked spectrum becomes the doublet one.

(iv) For a fixed κ , the effect of enlarging γ is only to reduce the heights of spikes in both two spectra and rarely changes the spectral profiles.

IV. CONCLUSION AND DISCUSSIONS

In this paper, we have investigated an atom-cavity system combined with an intracavity laser-driven parametric down-conversion. We considered two physical models with different atomic structures, the three-level Λ -type and ladder-type atomic configurations. In both composite systems, the intracavity laser-driven parametric oscillation works as a photon source and plays an important role in the collective atom-cavity dynamics. In the limit of the far-detuned atom-light field and atom-cavity interactions, both composite systems can be simplified to an effective spin-boson model, where a large number of two-level particles collectively interact with a single-mode cavity, via the adiabatic approximation.

We further map this spin-boson model into a two-mode boson model by employing the Holstein-Primakoff transformation. Based on the derived two-mode boson models, we investigated the potential phase transition in different systems to the second-order approximation in both nondissipative and dissipative cases. In addition, we have discussed the features of the light field leaking out of the optical resonator from aspects of cavity output-field spectra. The cavity dissipation provides us a way to monitor the collective atom-cavity dynamics and

the critical behavior and different properties of the system via various measurements on the output field.

In both composite systems, a superradiant phase transition is found via enlarging the system size N . The behaviors of the macroscopic occupation in the intracavity field (n_a) or the angular momentum of a pseudospin ensemble (n_b) versus N in different composite systems are alike. When N is larger than the critical system size N_c the intracavity photon number n_a strongly increases and then gradually falls. In contrast, the atomic excitation n_b always goes up and is saturated finally as N well exceeds N_c . This difference between the behaviors of n_a and n_b versus N can be interpreted from the fact of the N -dependent collective atom-cavity interaction.

Despite similarities, those two composite systems display some respective unique characteristics because of the different atomic structures.

For the Λ -type atomic system:

(i) Due to the extra nonlinear parametric processes, the counter-rotating wave interaction terms ($\hat{a}\hat{J}_-$ and $\hat{a}^+\hat{J}_+$), which play a significantly important role in the usual Dicke model [1], are presented in the spin-boson Hamiltonian [see Eq. (7)].

(ii) In the nondissipative case, only the atomic branch of the elementary excitation is valid in both normal and superradiant phases while the photonic branch is invalid.

(iii) In experiment, two lower atomic $|1\rangle$ and $|2\rangle$ states can be chosen as two ground-state hyperfine levels. In the limit of far-detuned atom-light field and atom-cavity interactions, the influence of the spontaneous emission of the upper atomic $|3\rangle$

state on the collective atom-cavity dynamics can be ignored. Thus, only the effect of the cavity loss is needed to be considered.

(iv) The behavior of the threshold N_c of the superradiant phase transition versus the cavity loss rate κ is completely different from the optical cavity QED system in Ref. [15]; i.e., N_c goes down as κ is increased.

For the ladder-type atomic system:

(i) No counter-rotating wave interaction terms exist in the spin-boson model, but the atomic ensemble interacts with a single-mode optical resonator via the two-photon transition [see Eq. (56)]. In this case, the collective atom-cavity interaction strength is enhanced by a factor of \sqrt{N} compared with the Λ -type system, which significantly reduces the critical system size N_c .

(ii) Since the spin-up $|3\rangle$ state in the spin-boson model [see Eq. (56)] must be an excited atomic level, the influence of the spontaneous emission of the $|3\rangle$ state on the collective atom-cavity dynamics cannot be ignored. Thus, the effects of both atomic spontaneous emission and cavity loss should be considered.

(iii) Unlike the Λ -type system, the threshold N_c of the superradiant phase transition goes up as the cavity loss rate is increased.

ACKNOWLEDGMENTS

D.Y. would like to thank Michael R. Hush for many useful discussions.

-
- [1] C. Emary and T. Brandes, *Phys. Rev. Lett.* **90**, 044101 (2003).
 [2] B. M. Garraway, *Philos. Trans. R. Soc., A* **369**, 1137 (2011).
 [3] P. Strack and S. Sachdev, *Phys. Rev. Lett.* **107**, 277202 (2011).
 [4] V. M. Bastidas, C. Emary, B. Regler, and T. Brandes, *Phys. Rev. Lett.* **108**, 043003 (2012).
 [5] S. Genway, W. Li, C. Ates, B. P. Lanyon, and I. Lesanovsky, *Phys. Rev. Lett.* **112**, 023603 (2014).
 [6] R. H. Dicke, *Phys. Rev.* **93**, 99 (1954).
 [7] K. Hepp and E. H. Lieb, *Ann. Phys.* **76**, 360 (1973).
 [8] Y. K. Wang and F. T. Hioe, *Phys. Rev. A* **7**, 831 (1973).
 [9] K. Baumann, C. Guerlin, F. Brennecke, and T. Esslinger, *Nature (London)* **464**, 1301 (2010).
 [10] K. Baumann, R. Mottl, F. Brennecke, and T. Esslinger, *Phys. Rev. Lett.* **107**, 140402 (2011).
 [11] J. Keeling, M. J. Bhaseen, and B. D. Simons, *Phys. Rev. Lett.* **105**, 043001 (2010).
 [12] P. Domokos and H. Ritsch, *Phys. Rev. Lett.* **89**, 253003 (2002).
 [13] D. Nagy, G. Szirmai, and P. Domokos, *Eur. Phys. J. D* **48**, 127 (2008).
 [14] P. Nataf and C. Ciuti, *Nat. Commun.* **1**, 72 (2010).
 [15] F. Dimer, B. Estienne, A. S. Parkins, and H. J. Carmichael, *Phys. Rev. A* **75**, 013804 (2007).
 [16] S. Gopalakrishnan, B. L. Lev, and P. M. Goldbart, *Phys. Rev. Lett.* **107**, 277201 (2011).
 [17] A. Baksic, P. Nataf, and C. Ciuti, *Phys. Rev. A* **87**, 023813 (2013).
 [18] M. Hayn, C. Emary, and T. Brandes, *Phys. Rev. A* **86**, 063822 (2012).
 [19] D. F. Walls and G. J. Milburn, *Quantum Optics* (Springer-Verlag, Berlin, 1994).
 [20] F. A. Montes and M. Xiao, *Phys. Rev. A* **62**, 023818 (2000).
 [21] M. G. A. Paris, *Phys. Lett. A* **217**, 78 (1996).
 [22] H. Katori, T. Ido, and M. Kuwata-Gonokami, *J. Phys. Soc. Jpn.* **68**, 2479 (1999).
 [23] T. Takekoshi, J. R. Yeh, and R. J. Knize, *Opt. Commun.* **114**, 421 (1995).
 [24] O. Madelung, *Introduction to Solid-State Theory* (Springer, Berlin, 1978).
 [25] C. Emary and T. Brandes, *Phys. Rev. A* **69**, 053804 (2004).
 [26] D. Nagy, G. Kónya, G. Szirmai, and P. Domokos, *Phys. Rev. Lett.* **104**, 130401 (2010).
 [27] C. Emary and T. Brandes, *Phys. Rev. E* **67**, 066203 (2003).
 [28] M. Tomka, D. Baeriswyl, and V. Gritsev, *Phys. Rev. A* **88**, 053801 (2013).
 [29] L. Davidovich, *Rev. Mod. Phys.* **68**, 127 (1996).
 [30] D. Yu and J. Chen, *Phys. Rev. A* **78**, 013846 (2008).
 [31] D. Yu and J. Chen, *Phys. Rev. A* **81**, 023818 (2010).
 [32] D. Yu and J. Chen, *Phys. Rev. A* **81**, 053809 (2010).
 [33] D. Yu and J. Chen, *Phys. Rev. A* **83**, 063846 (2011).
 [34] M. J. Collett and C. W. Gardiner, *Phys. Rev. A* **30**, 1386 (1984).
 [35] G. H. van Tartwijk and G. P. Agrawal, *Prog. Quantum Electron.* **22**, 43 (1998).
 [36] J. Berezovsky, M. H. Mikkelsen, O. Gywat, N. G. Stoltz, L. A. Coldren, and D. D. Awschalom, *Science* **314**, 1916 (2006).